A STUDY ON THE STRESS DISTRIBUTION AROUND ELLIPTICAL HOLES IN A FLAT PLATE SUBJECTED TO IN-PLANE LOADS

LT. (RHN) DEMOSTHENES HOZOS

COURSE XIII - A

MAY, 1969

A STUDY OF THE STRESS DISTRIBUTION AROUND ELLIPTICAL HOLES IN A FLAT PLATE SUBJECTED TO IN-PLANE LOADS

by

Demosthenes HOZOS
Lieutenant, Royal Greek Navy
B.S., Royal Greek Naval Academy

Submitted in Partial Fulfillment of the
Requirements for the Degree of
Master of Science in Naval Architecture
and Marine Engineering
at the
MASSACHUSETTS INSTITUTE OF TECHNOLOGY
May, 1969

TABLE OF CONTENTS

A STUDY OF THE STRESS DISTRIBUTION AROUND ELLIPTICAL HOLES IN A FLATE PLATE SUBJECTED TO IN-PLANE LOADS

by

Demosthenes HOZOS

ABSTRACT

A theoretical solution of the title problem was obtained and a computer program was developed to examine various geometric arrangements of elliptical holes in flat plates with different loading conditions.

Graphs of theoretical predictions are presented, discussed and compared with experimental results of other authors.

Thesis Supervisor: Norman Jones

Title: Assistant Professor of Naval Architecture

ACKNOWLEDGEMENTS

The author wishes to express his gratitude to Professor Norman Jones from whom most of the theoretical part of this work is drawn, for his extreme interest, encouragement, and advice as a thesis supervisor.

NOMENCLATURE

$2c$	Distance between the foci of the ellipses
a, b	Major and minor semiaxes of the elliptical hole
ξ, η	Elliptical coordinates of a point $P(x,y)$
ξ_0	Constant value of ξ of any point on the elliptical hole
Φ, X_i	Stress functions
σ_η	Normal stress intensity in the tangential direction to ξ = constant
σ_ξ	Normal stress intensity in the normal direction to ξ = constant
$\tau_{\xi\eta}$	Shear stress intensity
$\sigma_x, \sigma_y, \tau_{xy}$	The usual notation for stress intensities in Cartesian coordinates
W_x	Dimension of the plate in the x direction
W_y	Dimension of the plate in the y direction
$\lambda_x = \frac{2a}{W_x}$	
$\lambda_y = \frac{2b}{W_y}$	
σ_1	Uniformally distributed load applied on the edge $x = \frac{W_x}{2}$ and parallel to x axis
σ_2	Uniformally distributed load applied on the edge $y = \frac{W_y}{2}$ and parallel to y axis
a', b'	Semiaxes of the confocal ellipse $\xi = \xi_0$ passing through a point $P(x,y) \equiv P(\xi', \eta')$
SCF	Stress concentration factor = $\frac{\sigma_{max}}{\sigma_1}$ or $\frac{\sigma_{max}}{\sigma_2}$
SCF'	Stress concentration factor = $SCF \times (1-\lambda_x)$ or $SCF \times (1-\lambda_y)$

$\mu = b/a$ when loading parallel to the minor axis of the elliptical hole.

$\mu = a/b$ when loading parallel to the major axis of the elliptical hole.

INTRODUCTION

The behavior of thin flat elastic plates perforated with circular holes is well known for in-plane loading.

Theoretical methods and experimental results have been published by many authors. Refs. (1-7)

The case of one elliptical hole in an infinitely large plate is discussed in reference [1] for several loading conditions including the case where the major axis of the ellipse is inclined to the axis of the axial load.

Durelli and Murray [10] performed photoelastic tests on thin flat plates loaded with various combinations of biaxial stresses.

Durelli, Parks and Feng [9] examined cases of rectangular plates with one elliptical hole under axial loading, again using the photoelastic method.

The purpose of this study is to approach the problem theoretically and obtain results for the case of finite thin rectangular plates perforated with one elliptical hole and subjected to uniaxial or biaxial loading.

A computer program was developed and the published results of available experiments were used for comparison.

THEORY

The use of elliptical coordinates simplifies the mathematical analysis of the stresses around an elliptical hole in a flat plate loaded in the plane of the plate.

The equations of transformation from Cartesian to elliptical coordinates are

$$x = c \cdot \cosh \xi \cdot \cos \eta \tag{1}$$

$$y = c \cdot \sinh \xi \cdot \sin \eta \tag{2}$$

The conditions ξ = constant and η = constant are represented by a family of confocal ellipses and a family of confocal hyperbolae respectively, that are orthogonal and may be expressed as

$$\frac{x^2}{c^2 \cosh^2 \xi} + \frac{y^2}{c^2 \sinh^2 \xi} = 1 \tag{3}$$

$$\frac{x^2}{c^2 \cos^2 \eta} - \frac{y^2}{c^2 \sin^2 \eta} = 1 \tag{4}$$

Figure 1a represents the elliptical coordinates ξ, η of a point $P(x,y)$.

Using the notation

$$J^2 = \frac{c^2}{2}(\cosh 2\xi - \cos 2\eta) \tag{5}$$

the stress components can be expressed in elliptical coordinates in terms of a stress function Φ as

$$\sigma_\eta = \frac{1}{J^2}\frac{\partial^2\Phi}{\partial\xi^2} - \frac{\sinh\xi\cosh\xi}{J^2(\sin^2\eta+\sinh^2\xi)}\frac{\partial\Phi}{\partial\xi} + \\ - \frac{\sin\eta\cos\eta}{J^2(\sin^2\eta+\sinh^2\xi)}\frac{\partial\Phi}{\partial\eta} \tag{6}$$

$$\sigma_\xi = \frac{1}{J^2}\frac{\partial^2\Phi}{\partial\eta^2} - \frac{\sin\eta\cos\eta}{J^2(\sin^2\eta+\sinh^2\xi)}\frac{\partial\Phi}{\partial\eta} + \\ + \frac{\sinh\xi\cosh\xi}{J^2(\sin^2\eta+\sinh^2\xi)}\frac{\partial\Phi}{\partial\xi} \tag{7}$$

$$\tau_{\xi\eta} = -\frac{1}{J^2}\frac{\partial^2\Phi}{\partial\eta\partial\xi} + \frac{\sin\eta\cos\eta}{J^2(\sin^2\eta+\sinh^2\xi)}\frac{\partial\Phi}{\partial\xi} + \\ + \frac{\sinh\xi\cosh\xi}{J^2(\sin^2\eta+\sinh^2\xi)}\frac{\partial\Phi}{\partial\eta} \tag{8}$$

It is easy for one to verify that the expressions on page 538 in [4] reduce to equations (6), (7) and (8) above.

It might be noted here that the following assumptions have been made in the foregoing equations:

i. Isotropic elastic material

ii. Thin flat plate

iii. Infinitesimal deformations

The stress functions (9a-j) assumed here are the same as those which Coker and Filon used in reference [4]

$$X_1 = e^{(n+1)\xi}\cos\left[(n-1)\eta\right] + e^{(n-1)\xi}\cos\left[(n+1)\eta\right] \tag{9a}$$

$$X_2 = e^{-(n+1)\xi}\cos\left[(n-1)\eta\right] + e^{-(n-1)\xi}\cos\left[(n+1)\eta\right] \tag{9b}$$

$$X_3 = e^{(n+1)\xi}\sin\left[(n-1)\eta\right] + e^{(n-1)\xi}\sin\left[(n+1)\eta\right] \tag{9c}$$

$$X_4 = e^{-(n+1)\xi}\sin\left[(n-1)\eta\right] + e^{-(n-1)\xi}\sin\left[(n+1)\eta\right] \tag{9d}$$

$$X_5 = e^{n\xi}\cos n\eta \tag{9e}$$

$$X_6 = e^{-n\xi}\cos n\eta \tag{9f}$$

$$X_7 = e^{n\xi}\sin n\eta \tag{9g}$$

$$X_8 = e^{-n\xi} \sin n\eta \tag{9h}$$

$$X_9 = \xi \tag{9i}$$

$$X_{10} = \eta \tag{9j}$$

All the above functions satisfy the biharmonic equation for interger (or zero) values of n [4].

Equations (9a) through (9j) can be combined to give a general expression of the stress function

$$\begin{aligned}\Phi = {} & a_0\xi + b_0\eta + \sum_{n=0}^{\infty} \Big\{ c_n \left[e^{(n+1)\xi} \cos(n-1)\eta + e^{(n-1)\xi} \cos(n+1)\eta \right] + \\ & + d_n \left[e^{-(n-1)\xi} \cos(n-1)\eta + e^{-(n-1)\xi} \cos(n+1)\eta \right] + \\ & + e_n \left[e^{(n+1)\xi} \sin(n-1)\eta + e^{(n-1)\xi} \sin(n+1)\eta \right] + \\ & + f_n \left[e^{-(n+1)\xi} \sin(n-1)\eta + e^{-(n-1)\xi} \sin(n+1)\eta \right] + \\ & + g_n e^{n\xi} \cos n\eta + h_n e^{-n\xi} \cos n\eta + \\ & + j_n e^{n\xi} \sin n\eta + k_n e^{-n\xi} \sin n\eta \end{aligned} \tag{10}$$

When examinig the series with n=0 and n=1 then for finite stresses and displacements it is evident that the coefficients $d_o, f_o, h_o, j_o, k_o, f_1$ must equal zero.

The stress function given by equation (10) can be substituted in equations (6),(7),and (8) for the stresses.

However in the present analysis,only loading conditions that maintain symmetry about both the x and y axes are considered and therefore the coefficients of the terms that produce nonsymmetric functions of η for different values of n were set equal to zero.

Finally the stresses from (6),(7) and (8) have the form:

$$\frac{4J^4}{c^2}\,\sigma_\xi = \sum_{n=1,3,\ldots}^{\infty} n \left\{ \left[C_n (n+1) e^{(n-1)\xi} + D_n (n+1) e^{-(n-1)\xi} \right] \cos(n+3)\eta + \right.$$

$$+ \left[-4 C_n e^{(n+1)\xi} - C_n (n+3) e^{(n-3)\xi} - 4 D_n e^{-(n+1)\xi} - \right.$$

$$\left. - D_n (n+3) e^{-(n-3)\xi} \right] \cos(n+1)\eta +$$

$$+ \left[4 C_n e^{(n-1)\xi} - C_n (n-3) e^{(n+3)\xi} + 4 D_n e^{-(n-1)\xi} - \right.$$

$$\left. - D_n (n-3) e^{-(n+3)\xi} \right] \cos(n-1)\eta +$$

$$\left. + \left[C_n (n-1) e^{(n+1)\xi} + D_n (n-1) e^{-(n+1)\xi} \right] \cos(n-3)\eta \right\} +$$

$$+\sum_{n=2,4\ldots}^{\infty} n\Big\{\Big[G_n(n-1)e^{n\xi}+H_n(n-1)e^{-n\xi}\cos(n+2)\eta+$$

$$+\Big[-G_n(n-1)e^{(n+2)\xi}-G_n(n+1)e^{(n-2)\xi}-H_n(n-1)e^{-(n+2)\xi}-$$

$$-H_n(n+1)e^{-(n-2)\xi}\Big]\cos n\eta+$$

$$+\Big[G_n(n+1)e^{n\xi}+H_n(n+1)e^{-n\xi}\Big]\cos(n-2)\eta+$$

$$+2A_o\sinh 2\xi \qquad (11)$$

$$\frac{4J^4}{c^2}\sigma_\eta=\sum_{n=1,3\ldots}^{\infty} n\Big\{\Big[-C_n(n-3)e^{(n-1)\xi}-D_n(n-3)e^{-(n-1)\xi}\Big]\cos(n+3)\eta+$$

$$+\Big[-4C_n e^{(n+1)\xi}+C_n(n-1)e^{(n-3)\xi}-4D_n e^{-(n+1)\xi}+$$

$$+D_n(n-1)e^{-(n-3)\xi}\Big]\cos(n+1)\eta+$$

$$+\Big[4C_n e^{(n-1)\xi}+C_n(n+1)e^{(n+3)\xi}+4D_n e^{-(n-1)\xi}+$$

$$+D_n(n+1)e^{-(n+3)\xi}\Big]\cos(n-1)\eta+$$

$$\Big[-C_n(n+3)e^{(n+1)\xi}-D_n(n+3)e^{-(n+1)\xi}\Big]\cos(n-3)\eta+$$

$$+\sum_{n=2,4\ldots}^{\infty} n\Big\{\Big[-G_n(n-1)e^{+n\xi}-H_n(n-1)e^{-n\xi}\Big]\cos(n+2)\eta+$$

$$+\left[G_n(n-1)e^{(n+2)\xi} + G_n(n+1)e^{(n-2)\xi} + H_n(n-1)e^{-(n+2)\xi} + \right.$$

$$\left. + H_n(n+1)e^{-(n-2)\xi}\right]\cos n\eta +$$

$$+\left[-G_n(n+1)e^{n\xi} - H_n(n+1)e^{-n\xi}\right]\cos(n-2)\eta \Big\} -$$

$$-2A_0 \sinh 2\xi \qquad (12)$$

$$\frac{4J^4}{c^2}\tau_{\xi\eta} = \sum_{n=1,3\ldots}^{\infty} n\left\{\left[-C_n(n-1)e^{(n-1)\xi} + D_n(n-1)e^{-(n-1)\xi}\right]\sin(n+3)\eta + \right.$$

$$+\left[C_n(n+1)e^{(n-3)\xi} - D_n(n+1)e^{-(n-3)\xi}\right]\sin(n+1)\eta +$$

$$+\left[C_n(n-1)e^{(n+3)\xi} - D_n(n-1)e^{-(n+3)\xi}\right]\sin(n-1)\eta +$$

$$\left. +\left[-C_n(n+1)e^{(n+1)\xi} + D_n(n+1)e^{-(n+1)\xi}\right]\sin(n-3)\eta\right\} +$$

$$+ \quad n\left\{\left[-G_n(n-1)e^{n\xi} + H_n(n-1)e^{-n\xi}\right]\sin(n+2)\eta + \right.$$

$$+\left[G_n(n-1)e^{(n+2)\xi} + G_n(n+1)e^{(n-2)\xi} - H_n(n-1)e^{-(n+2)\xi} - \right.$$

$$\left. -H_n(n+1)e^{-(n-2)\xi}\right]\sin n\eta + \left[-G_n(n+1)e^{n\xi} + \right.$$

$$\left. + H_n(n+1)e^{-n\xi}\right]\sin(n-2)\eta + 2A_0 \sin 2\eta \qquad (13)$$

However equations (11), (12) and (13) are rearranged, in Appendix 1, in a more suitable form for translation into computer language.

The normal and shear stress components in Cartesian coordinates can be computed from the equations:

$$\sigma_x = \sigma_\eta \cos^2\alpha + \sigma_\xi \sin^2\alpha - \tau_{\xi\eta} \sin 2\alpha \qquad (14)$$

$$\sigma_y = \sigma_\eta \sin^2\alpha + \sigma_\xi \cos^2\alpha + \tau_{\xi\eta} \sin 2\alpha \qquad (15)$$

$$\tau_{xy} = \frac{1}{2} (\sigma_\xi - \sigma_\eta) \sin 2\alpha - \tau_{\xi\eta} \cos 2\alpha \qquad (16)$$

where

$$\cos\alpha = \frac{\sqrt{2} \cosh\xi \sin\eta}{\sqrt{\cosh 2\xi - \cos 2\eta}} \qquad (17)$$

$$\sin\alpha = \frac{\sqrt{2} \sinh\xi \cos\eta}{\sqrt{\cosh 2\xi - \cos 2\eta}} \qquad (18)$$

Equations (14), (15) and (16) are derived as usual from equilibrium conditions on an element. (Fig. 1b)

BOUNDARY CONDITIONS

Equations (11), (12) and (13) satisfy the required conditions of symmetry and antisymmetry refered to in the previous section. In addition to this σ_ξ and $\tau_{\xi\eta}$ must vanish at $\xi = \xi_0$. Page 198, [1]

Therefore at each point on the elliptical hole we must satisfy

$$\sigma_\xi = 0 \quad ; \quad \xi = \xi_0 \tag{19a}$$

$$\tau_{\xi\eta} = 0 \quad ; \quad \xi = \xi_0 \tag{19b}$$

For the case of one elliptical hole in an elastic finite flat rectangular plate loaded biaxially we must satisfy the following two conditions (20) and (21), in addition to (19)

$$\tau_{xy} = 0 \tag{20a}$$

$$\sigma_y = \sigma_2 \quad ; \quad Y = \frac{W_y}{2} \tag{20b}$$

$$\tau_{xy} = 0 \tag{21a}$$

$$\sigma_x = \sigma_1 \quad ; \quad X = \frac{W_x}{2} \tag{21b}$$

Due to the symmetry about both the x and y axes it is enough to examine only one quadrant of the plate.

Figure 2 illustrates all the cases under consideration. The numbers appearing in parentheses are the numbers of the equations of the boundary conditions applied for each particular case.

NUMERICAL METHOD

Initially the number of unknown constants appearing in equations (11) up to (13) was determined by an arbitrary truncation of the series.

Later the behavior of the series was examined for several cases and it was realized that the series doesn't always behave well. Similar convergence problems for functions involving elliptical coordinates were pointed out in reference [6]

In this case, the reason is believed to be the very rapid convergence of the coefficients of Dn and Hn after the fifth or sixth term, resulting in a very rapid divergence of the coefficients of Cn and Gn for all of the cases that were examined.

Finally twenty terms plus the constant term of the series were chosen.

Using the Overdetermined Collocation method (Ref. 8) the following cases were examined:

a.- Six fixed points on the inner boundary and another six fixed points on the outer boundary were selected to satisfy the boundary conditions. (Fig.2d)

b.- Decreasing by one the number of points on the ellipse with no change on the outer edges produced no difference in the numerical results obtained in case (α).

c.- With six points on the ellipse and eight on the outer boundary, the shape of the curve for the tangential stress distribution around the elliptical hole was changed to a flatter one and it was realized that the boundary conditions

were not satisfied as well as before due to the least squares process involved in the numerical method.

d.- The case of five points on the inner boundary and eight on the outer one was examined and it was found that the error introduced was smaller than in case (c), but not as small as in cases (a) and (b). (Verifying the satisfaction of the boundary conditions)

It might be noted here that a smaller number of points than in case (a) was used by Christiansen [15] for a similar problem.

For the case of axial loading parallel to the minor axis of the ellipse and for values of $\lambda_x < 0.5$ (wide plate) the expression ξ approaches infinity and no results could be obtained (Appendix 1).

The same effect happens for the case when plates with $\lambda_y > 0.5$ are loaded parallel to the major axis of the elliptical hole.

From the boundary conditions a set of M linear algebraic equations in N unknowns is formed, where $M > N$.

In matrix notation

$$AX = B \qquad (22)$$

where A is the M by N matrix of the coefficients of the unknown constants X.

By means of a least-squares method the normal equations

are obtained and the system in matrix notation has the form

$$\overset{T}{A}AX = \overset{T}{A}B \qquad (23)$$

These normal equations are solved by elimination using largest pivotal divisor [Ref. 12]

A computer program was developed and written in FORTRAN IV to execute all the required steps and calculate the tangential stress σ_η around the ellipse and the normal stresses along the axes of symmetry of the plate.

Subroutines for matrix operation are taken from reference [12]

All the necessary calculations for the problems under consideration are carried out by the same computer program by transfering control to the proper boundary conditions.

The required input information for each plate to be examined, must be typed on one card and many plates can be analyzed the same time.

Details for the input cards are given on comment cards in the program.

Additional details about the problem formulation are given in Appendix 1.

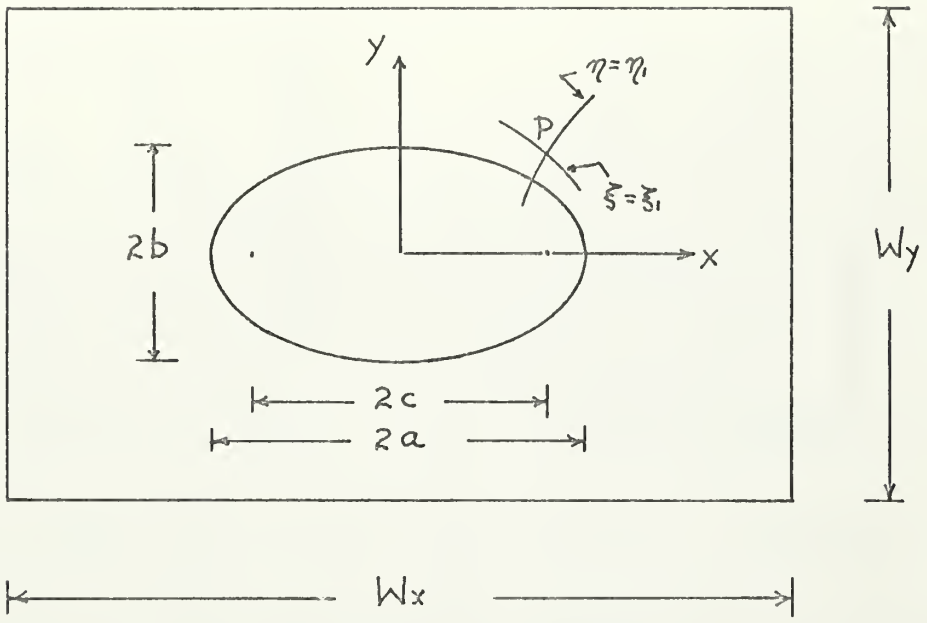

(a)

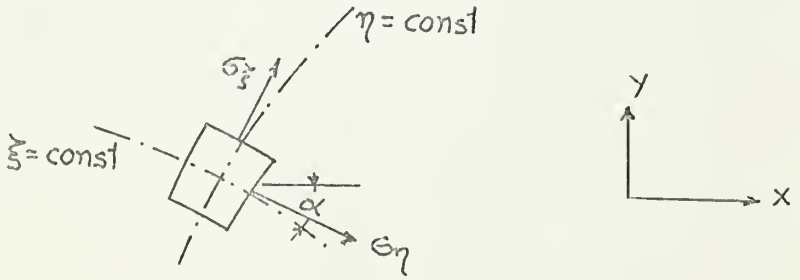

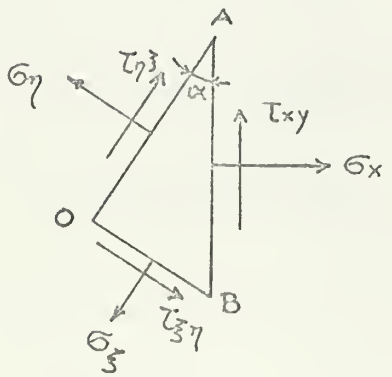

(AB) = 1

(OA) = cos α

(OB) = sin α

(b)

FIG 1

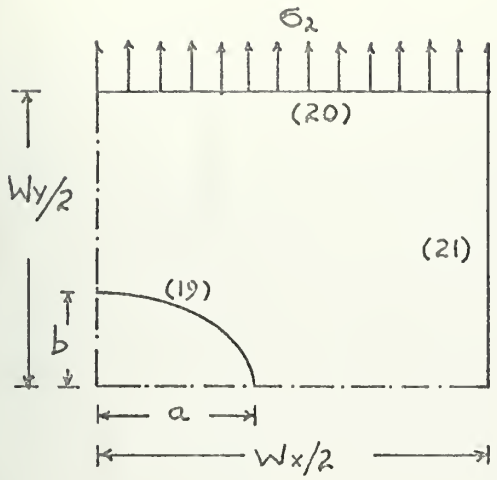
σ2
(20)
Wy/2
(21)
(19)
b
a
Wx/2

(a)

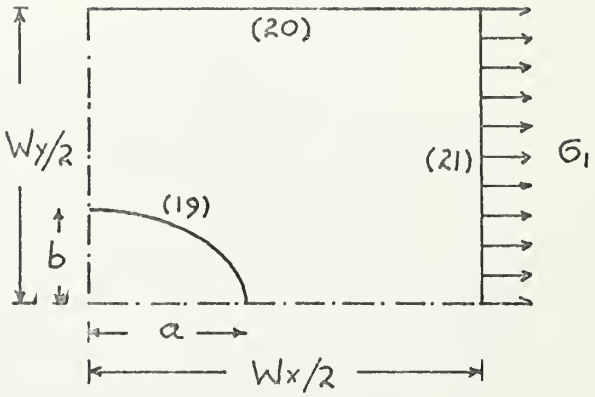
(20)
Wy/2
(21)
σ1
(19)
b
a
Wx/2

(b)

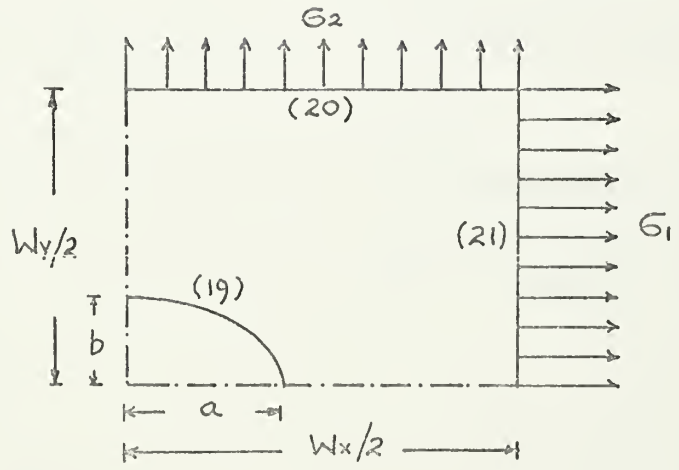
σ2
(20)
Wy/2
(21)
σ1
(19)
b
a
Wx/2

(c)

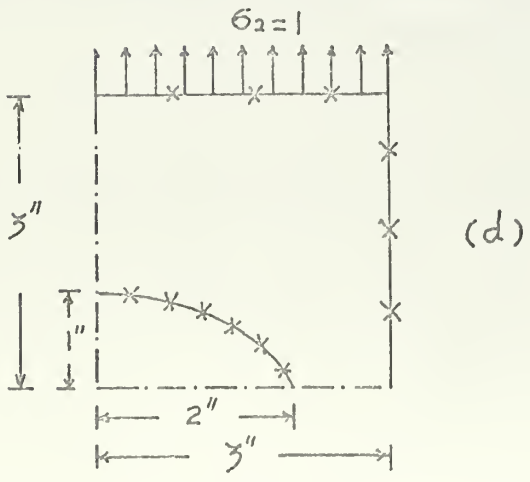
σ2=1
3"
1"
2"
3"

(d)

FIG 2

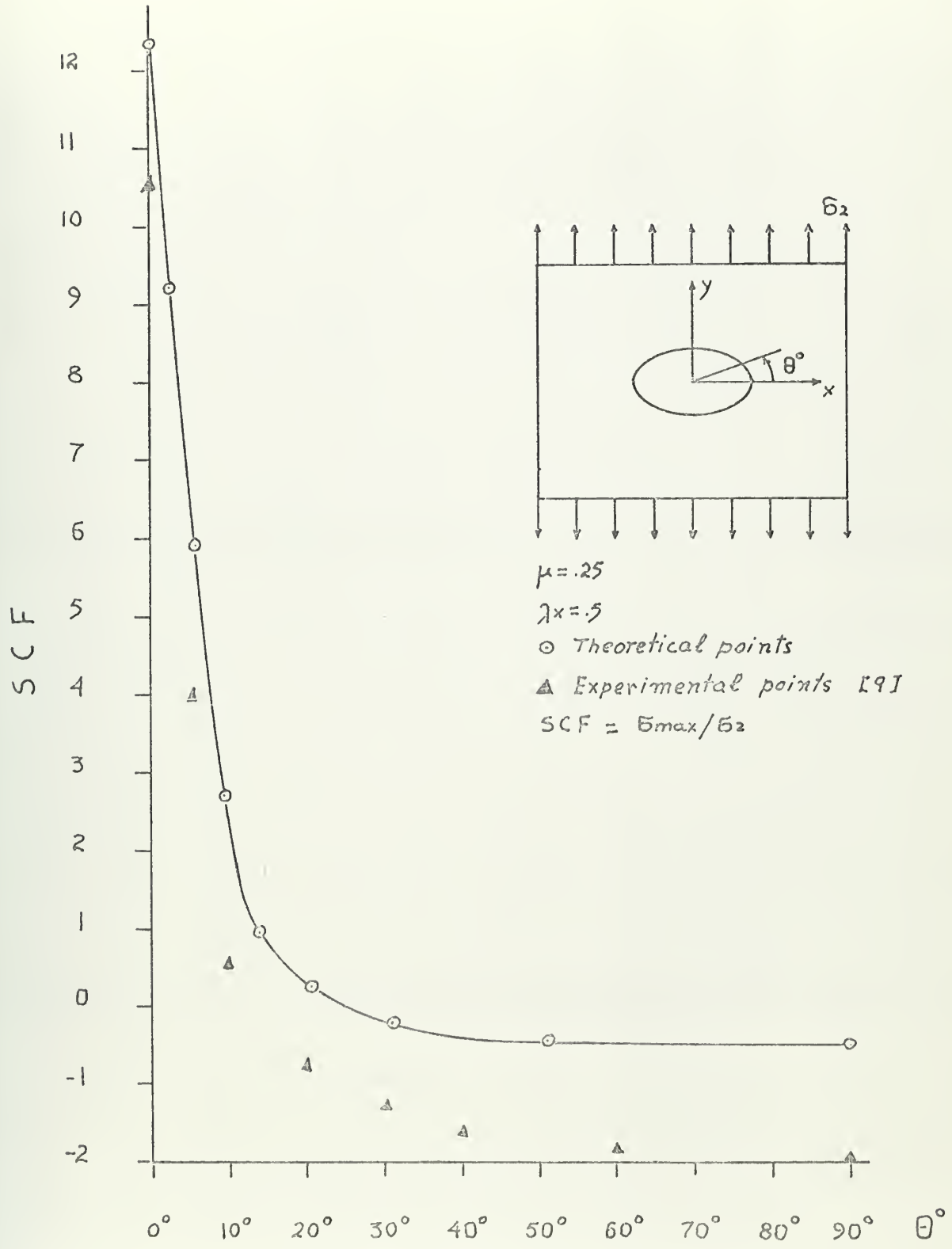
SCF
12
11
10
9
8
7
6
5
4
3
2
1
0
-1
-2
0°
10°
20°
30°
40°
50°
60°
70°
80°
90°
Θ°
σ2
y
θ°
x
μ = .25
λx = .5
⊙ Theoretical points
▲ Experimental points [9]
SCF = σmax/σ2

FIG 3

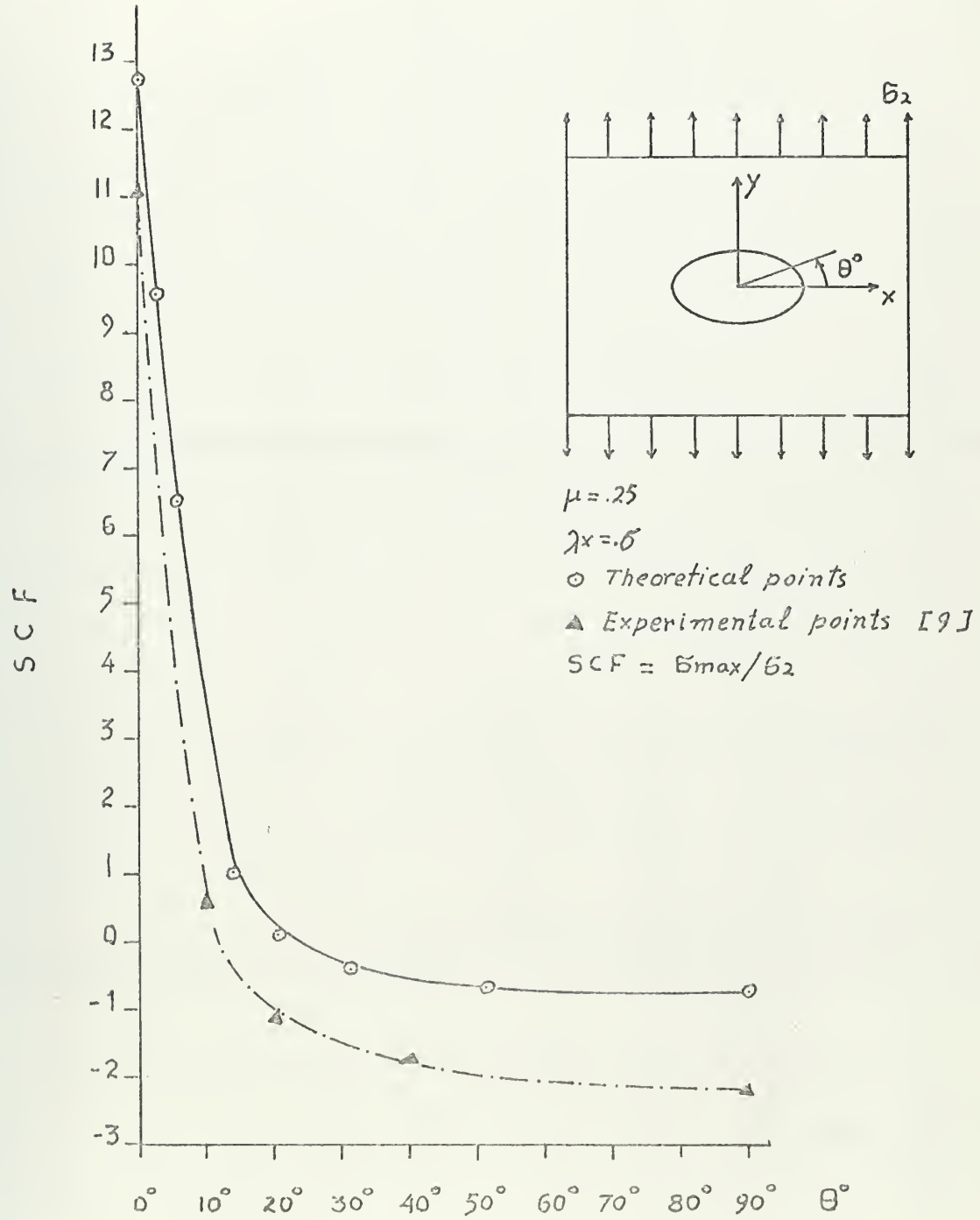
SCF
13
12
11
10
9
8
7
6
5
4
3
2
1
0
-1
-2
-3
0°
10°
20°
30°
40°
50°
60°
70°
80°
90°
θ°
σ2
y
θ°
x
μ = .25
λx = .6
⊙ Theoretical points
▲ Experimental points [9]
SCF = σmax/σ2

FIG 4

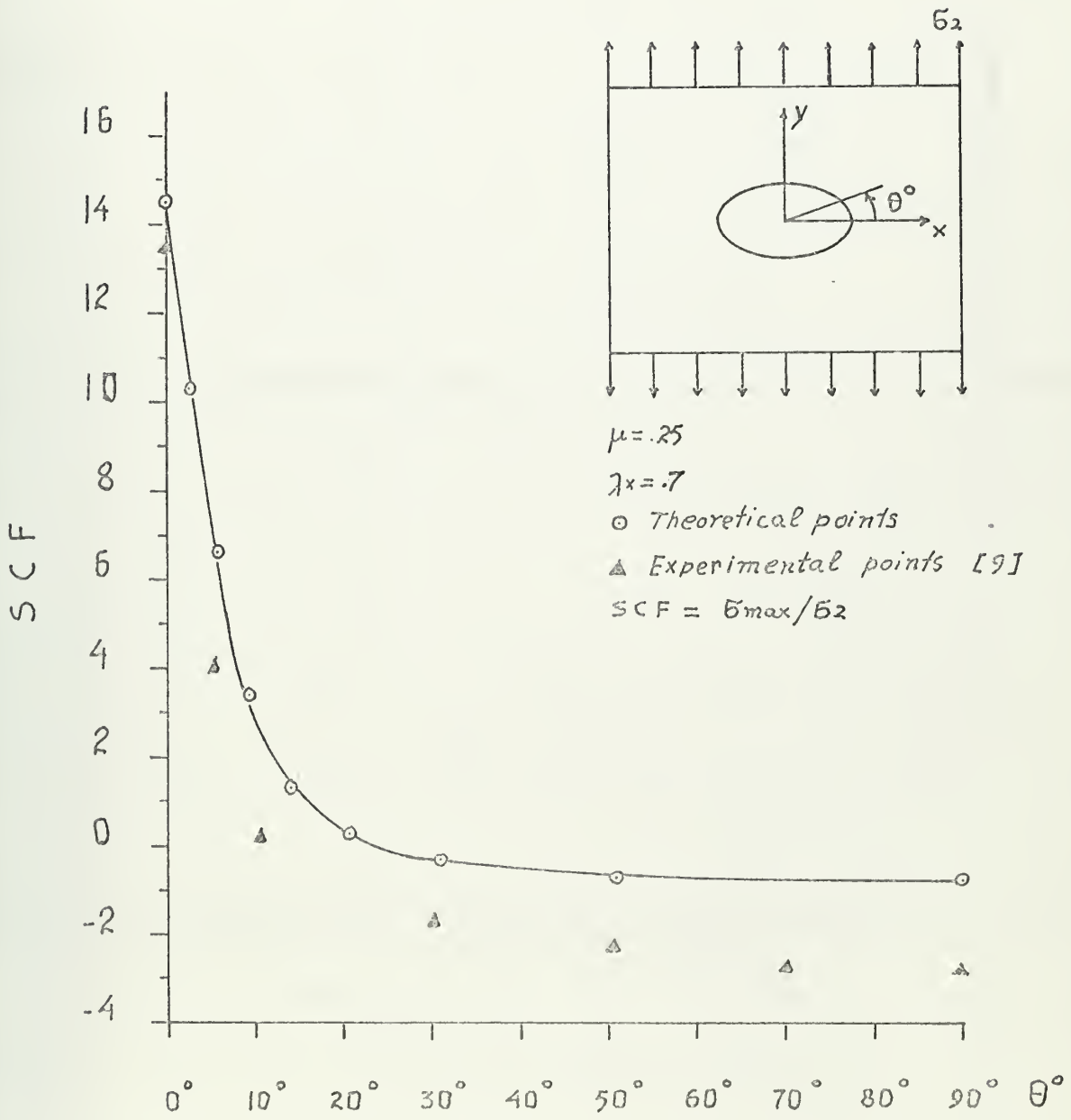
σ2
y
θ°
x
μ=.25
λx=.7
⊙ Theoretical points
▲ Experimental points [9]
SCF = σmax/σ2
SCF
16
14
12
10
8
6
4
2
0
-2
-4
0°
10°
20°
30°
40°
50°
60°
70°
80°
90°
θ°

FIG 5

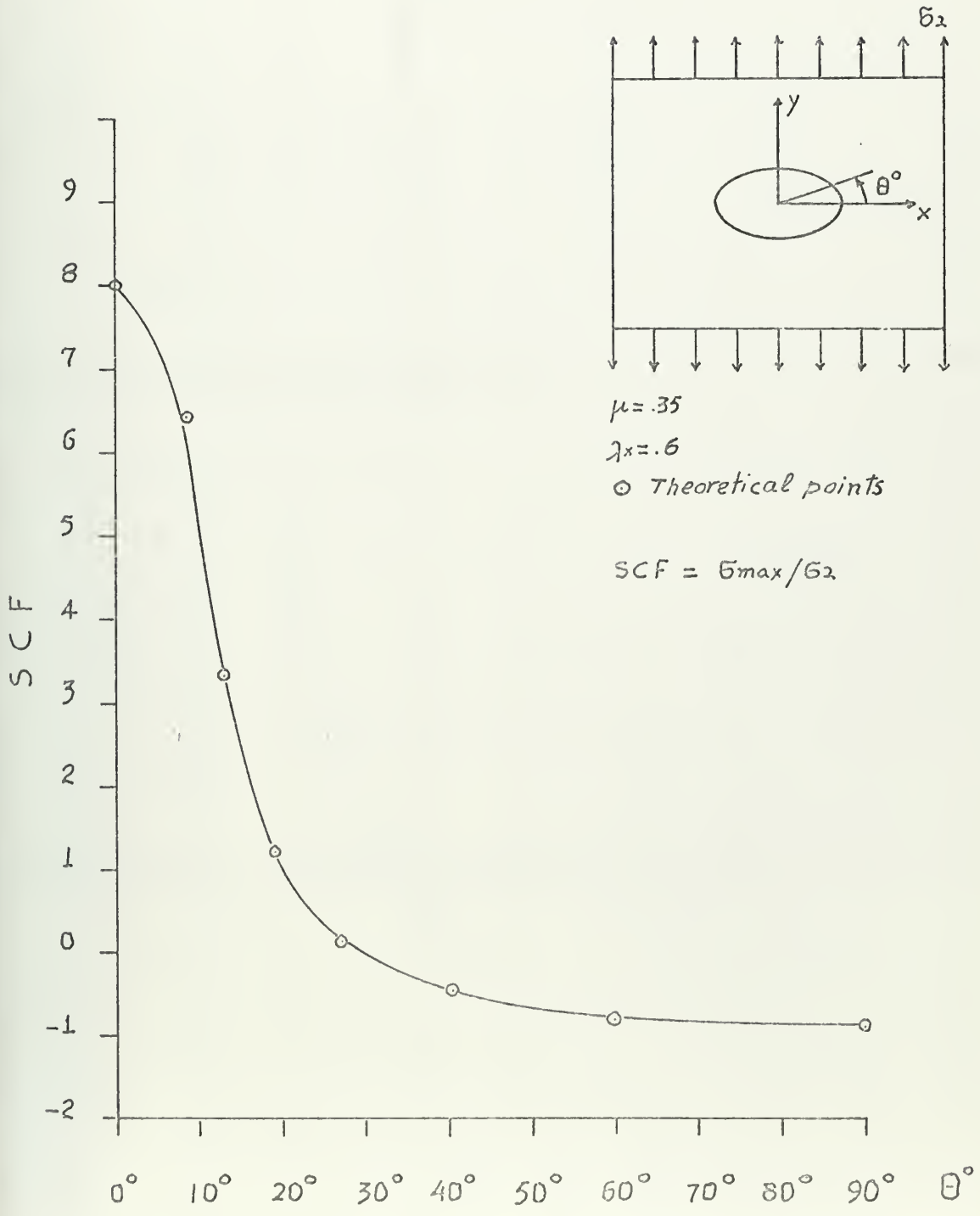
σ2
y
θ°
x
μ = .35
λx = .6
⊙ Theoretical points
SCF = σmax/σ2
SCF
9
8
7
6
5
4
3
2
1
0
-1
-2
0°
10°
20°
30°
40°
50°
60°
70°
80°
90°
θ°

FIG 6

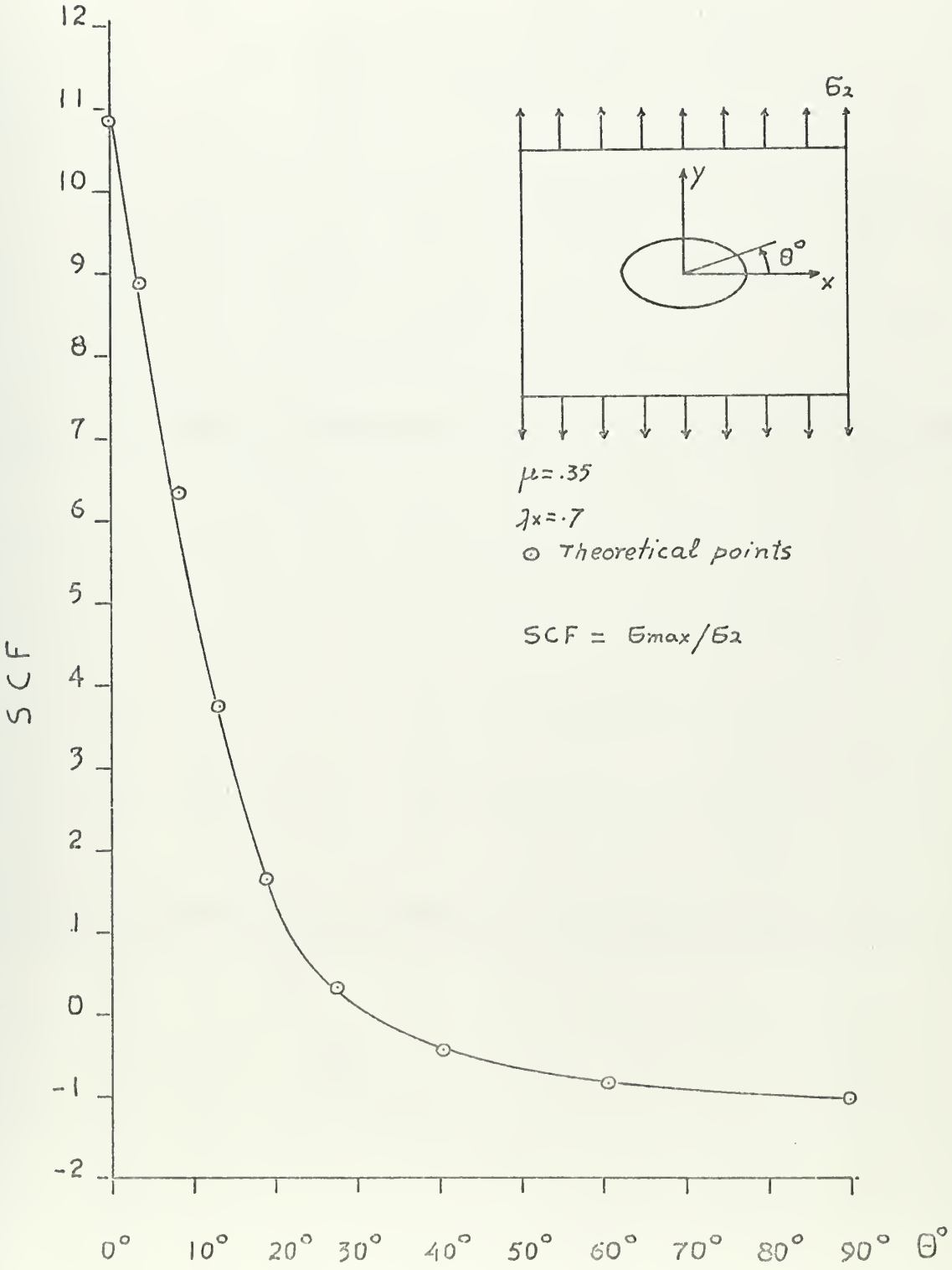
12
11
10
9
8
7
6
5
4
3
2
1
0
-1
-2
SCF
0°
10°
20°
30°
40°
50°
60°
70°
80°
90°
θ°
σ2
y
θ°
x
μ=.35
γx=.7
⊙ Theoretical points
SCF = σmax/σ2

FIG 7

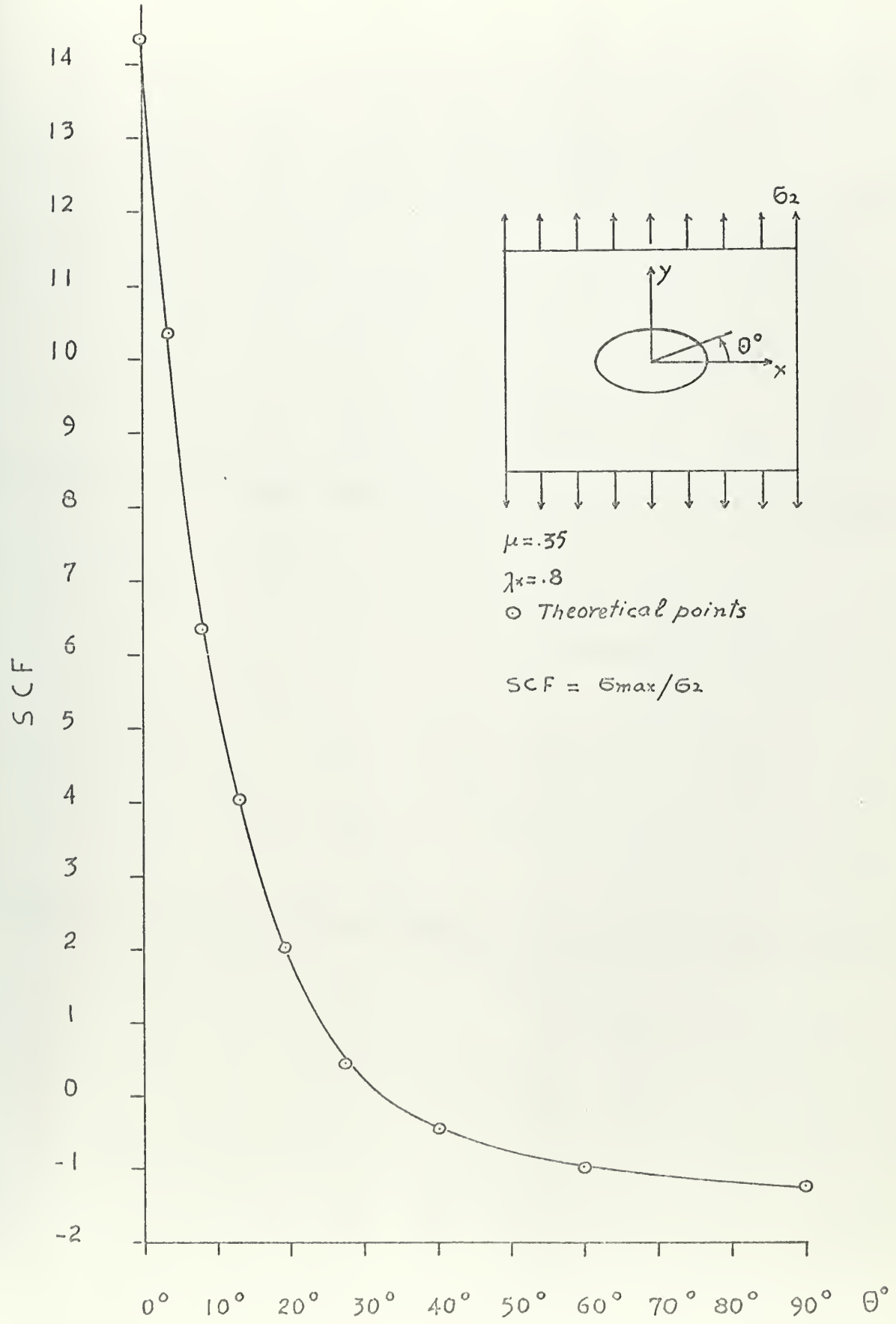
SCF
14
13
12
11
10
9
8
7
6
5
4
3
2
1
0
-1
-2
0°
10°
20°
30°
40°
50°
60°
70°
80°
90°
θ°
σ2
y
θ°
x
μ=.35
λx=.8
⊙ Theoretical points
SCF = σmax/σ2

FIG 8

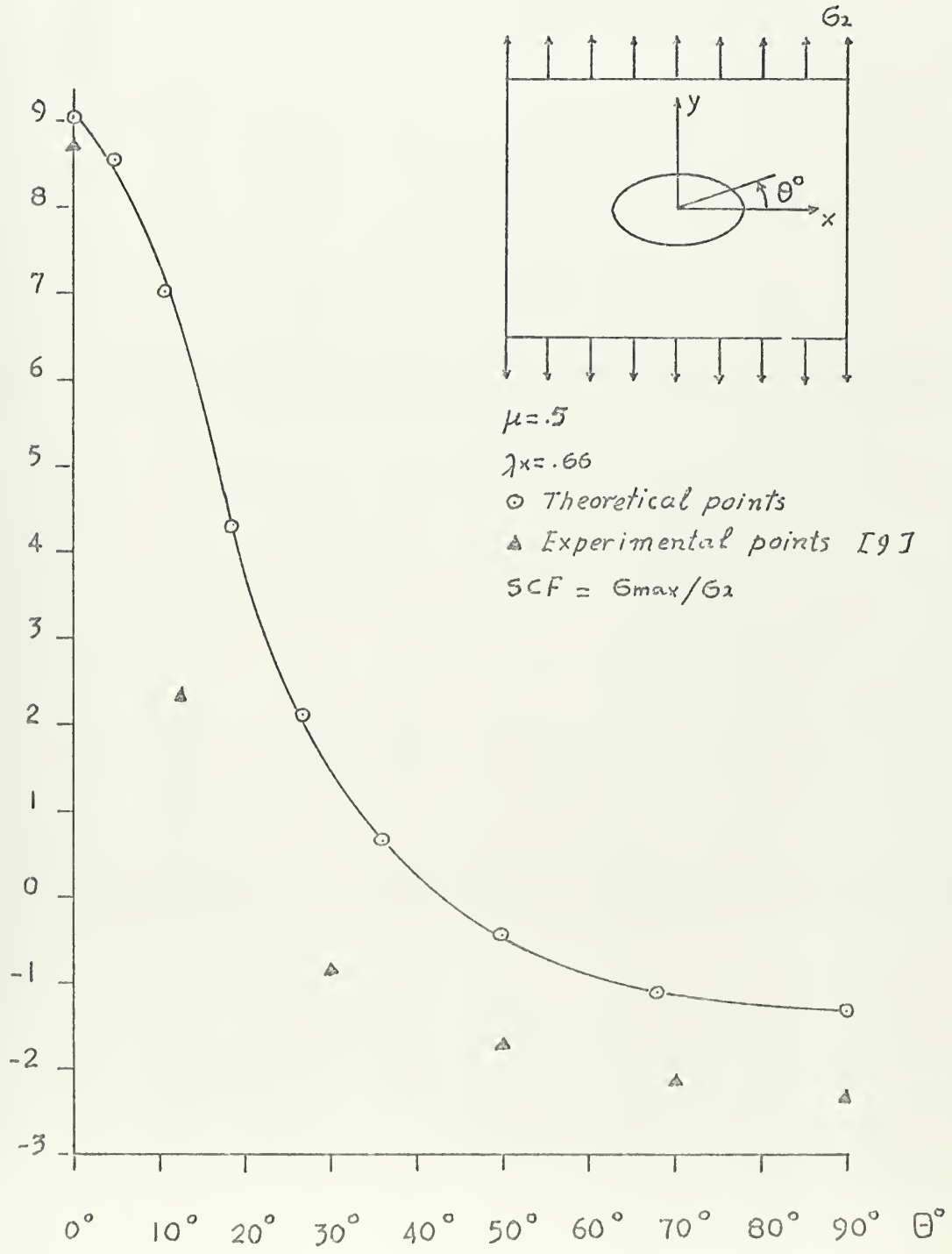
σ2
y
θ°
x
μ=.5
λx=.66
⊙ Theoretical points
▲ Experimental points [9]
SCF = σmax/σ2
9
8
7
6
5
4
3
2
1
0
-1
-2
-3
0°
10°
20°
30°
40°
50°
60°
70°
80°
90°
Θ°

FIG 9

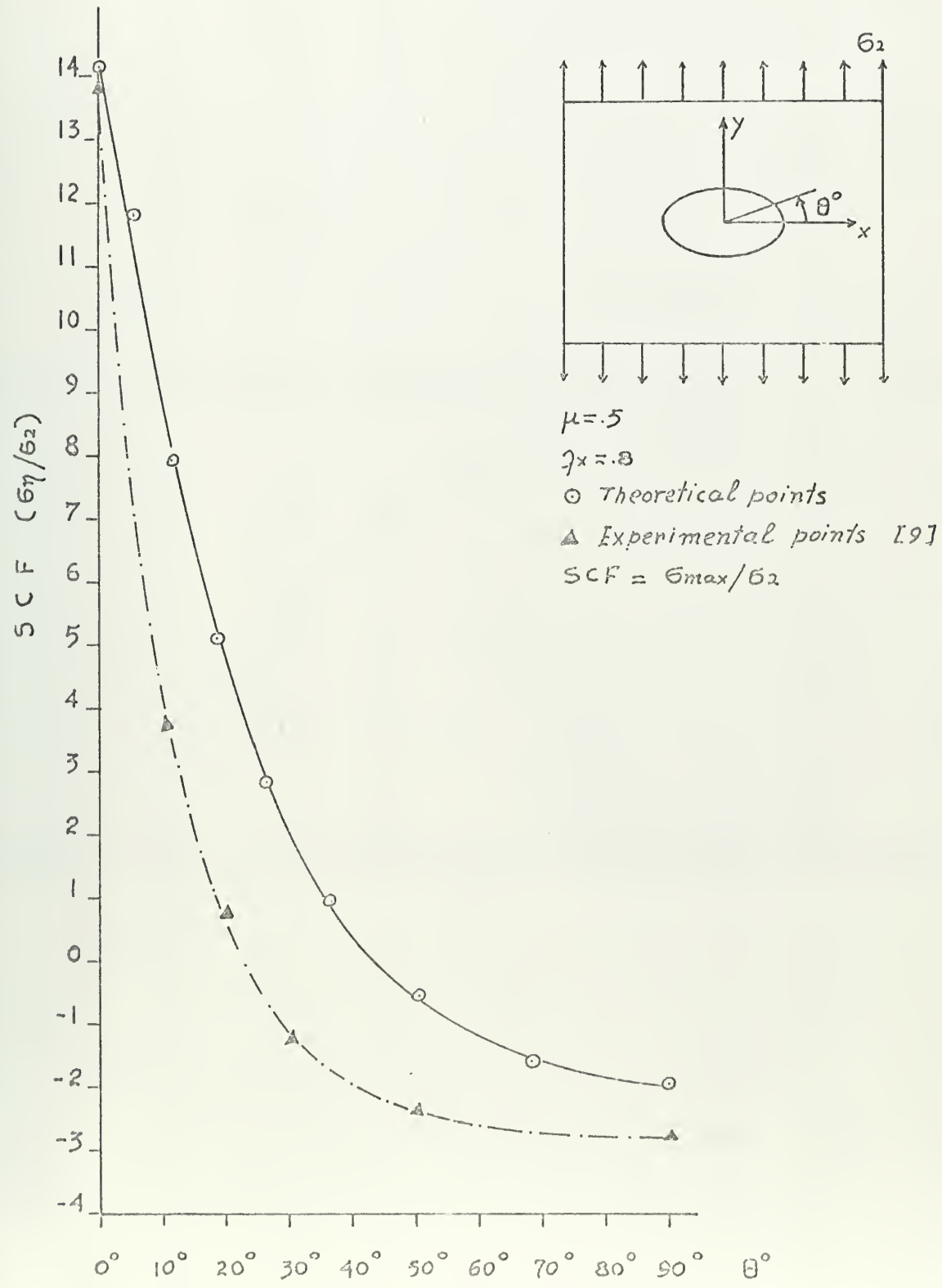
SCF (ση/σ2)
14
13
12
11
10
9
8
7
6
5
4
3
2
1
0
-1
-2
-3
-4
0° 10° 20° 30° 40° 50° 60° 70° 80° 90° θ°
σ2
y
θ°
x
μ=.5
ηx=.8
⊙ Theoretical points
▲ Experimental points [9]
SCF = σmax/σ2

FIG 10

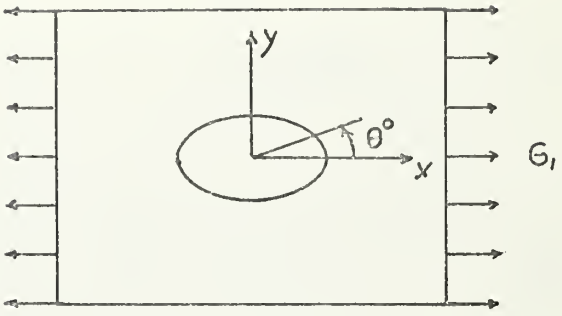
y
θ°
x
σ1

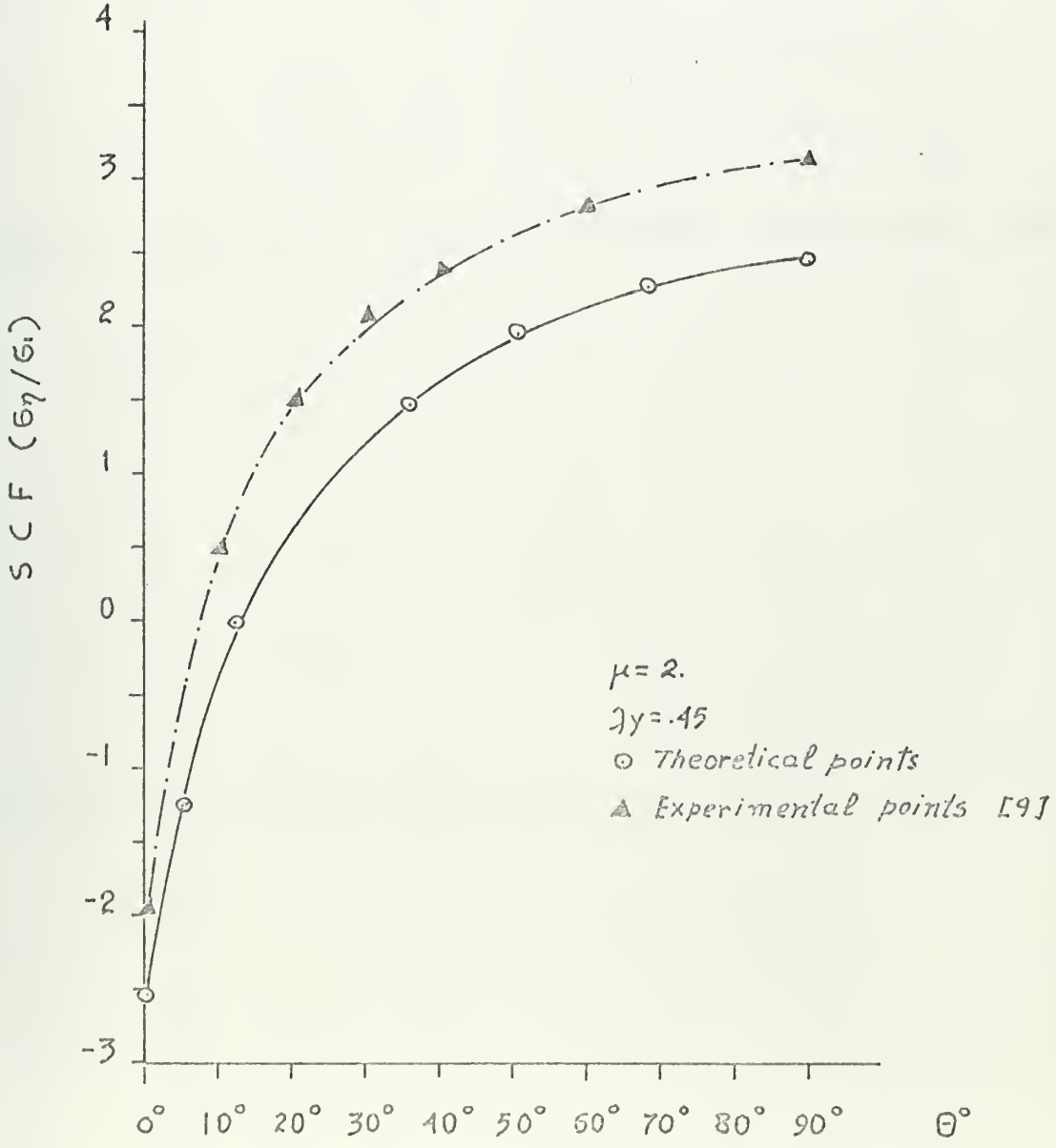
SCF (ση/σ1)
4
3
2
1
0
-1
-2
-3
0° 10° 20° 30° 40° 50° 60° 70° 80° 90°
θ°
μ = 2.
ηy = .45
Theoretical points
Experimental points [9]

FIG 11

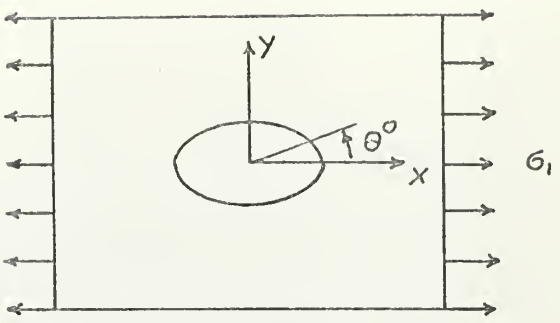
y
θ°
x
σ1

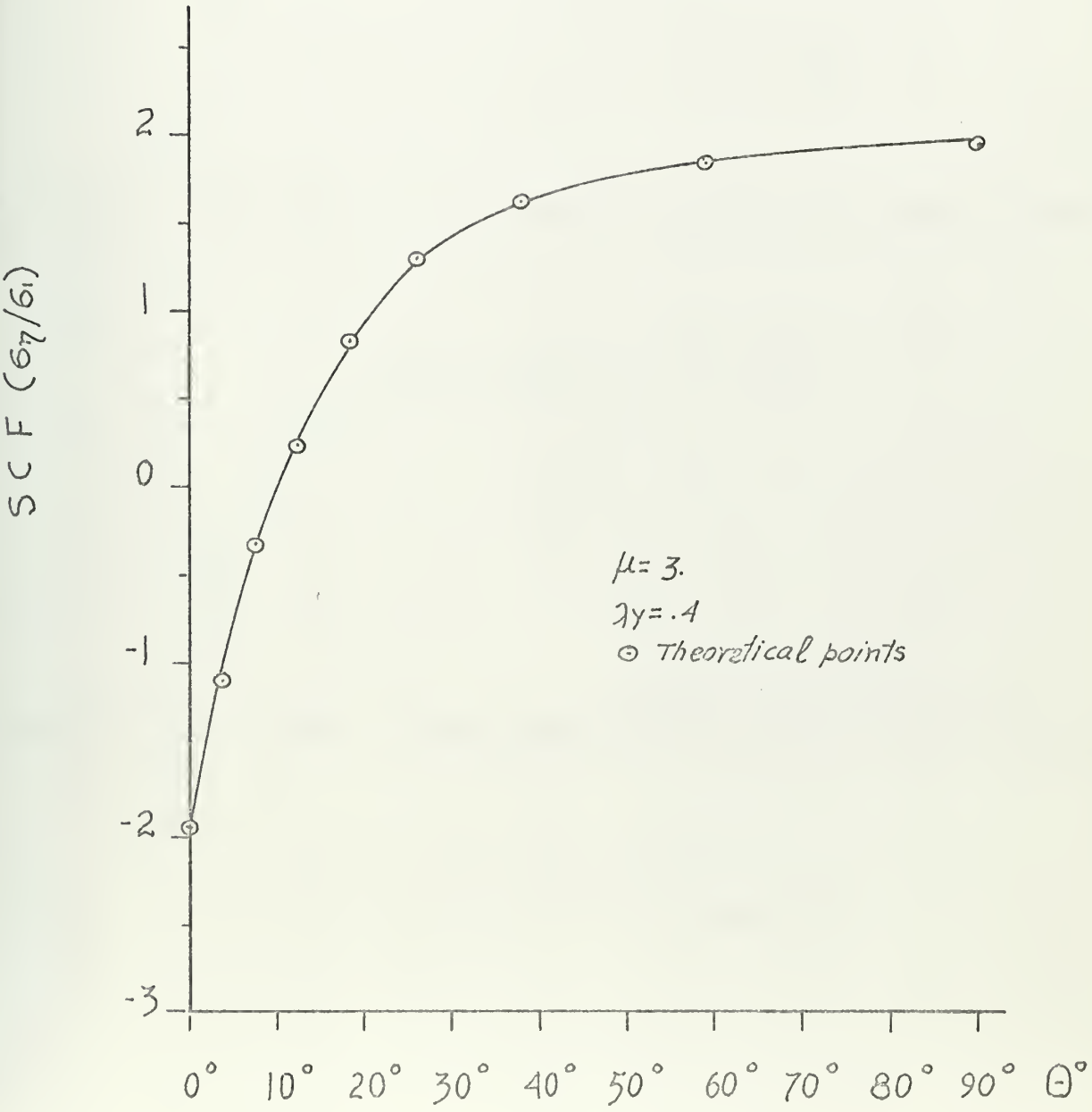
SCF (σ7/σ1)
2
1
0
-1
-2
-3
0° 10° 20° 30° 40° 50° 60° 70° 80° 90° θ°
μ= 3.
λy= .4
⊙ Theoretical points

FIG 12

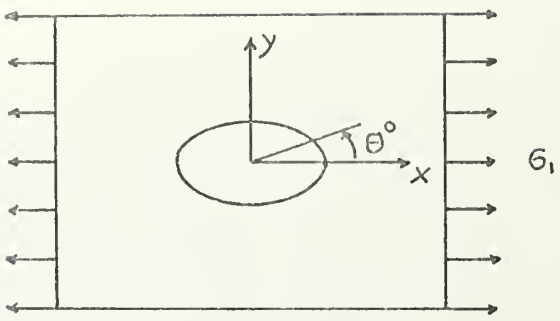
y
θ°
x
σ1

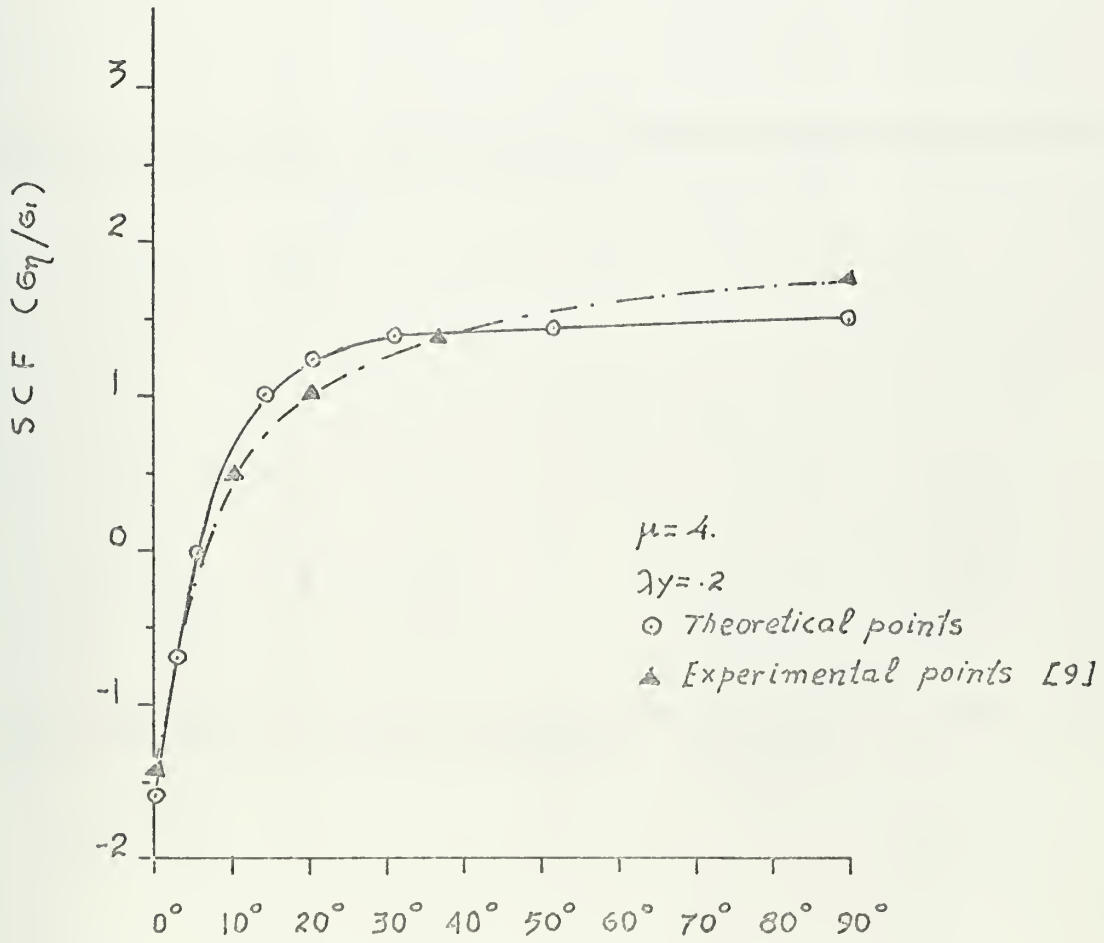
SCF (ση/σ1)
3
2
1
0
-1
-2
0° 10° 20° 30° 40° 50° 60° 70° 80° 90°
μ=4.
λy=.2
Theoretical points
Experimental points [9]

FIG 13

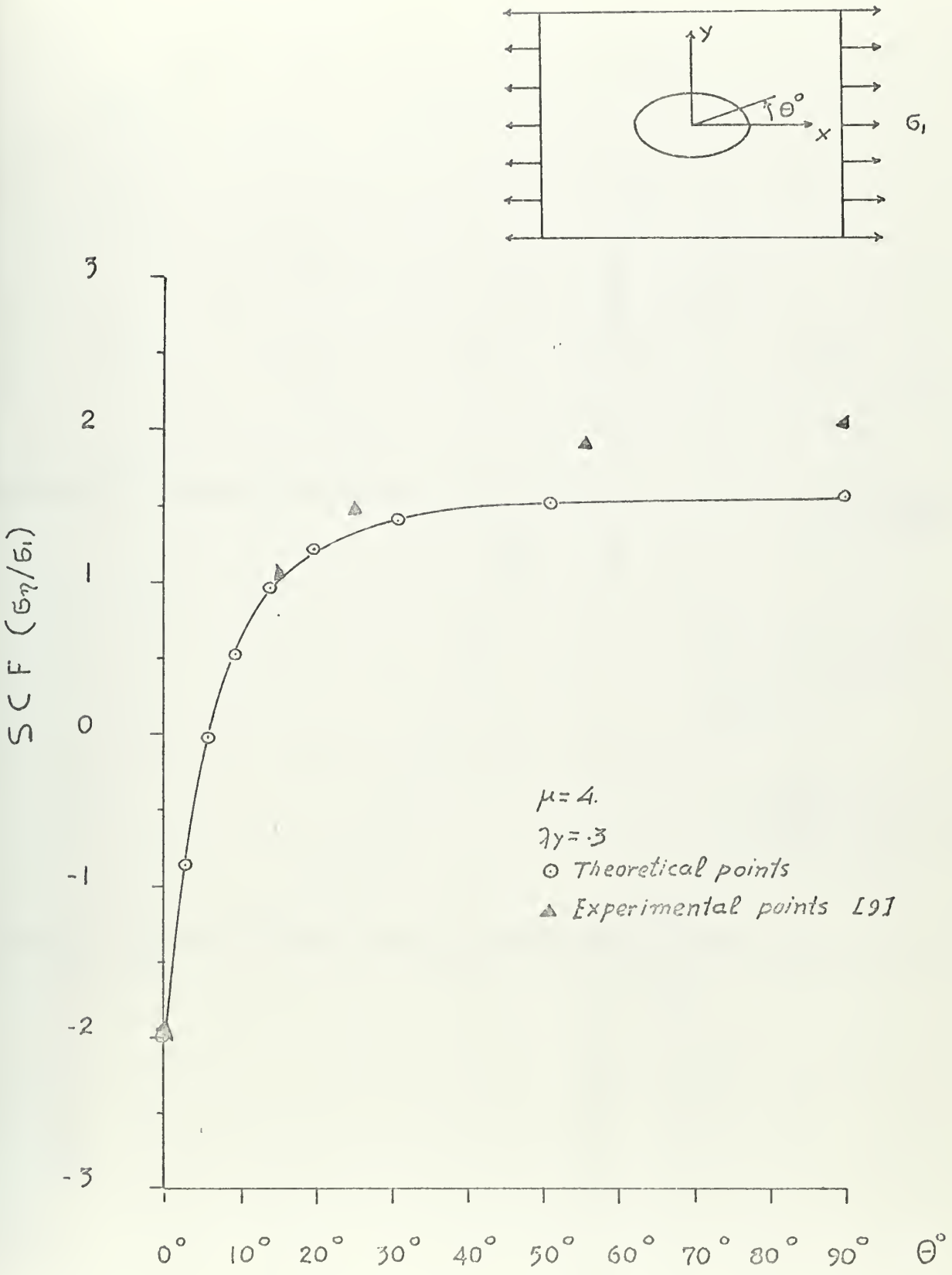
y
θ°
x
σ1
SCF (σθ/σ1)
3
2
1
0
-1
-2
-3
μ = 4.
λy = .3
Theoretical points
Experimental points [9]
0°
10°
20°
30°
40°
50°
60°
70°
80°
90°
θ°

FIG 14

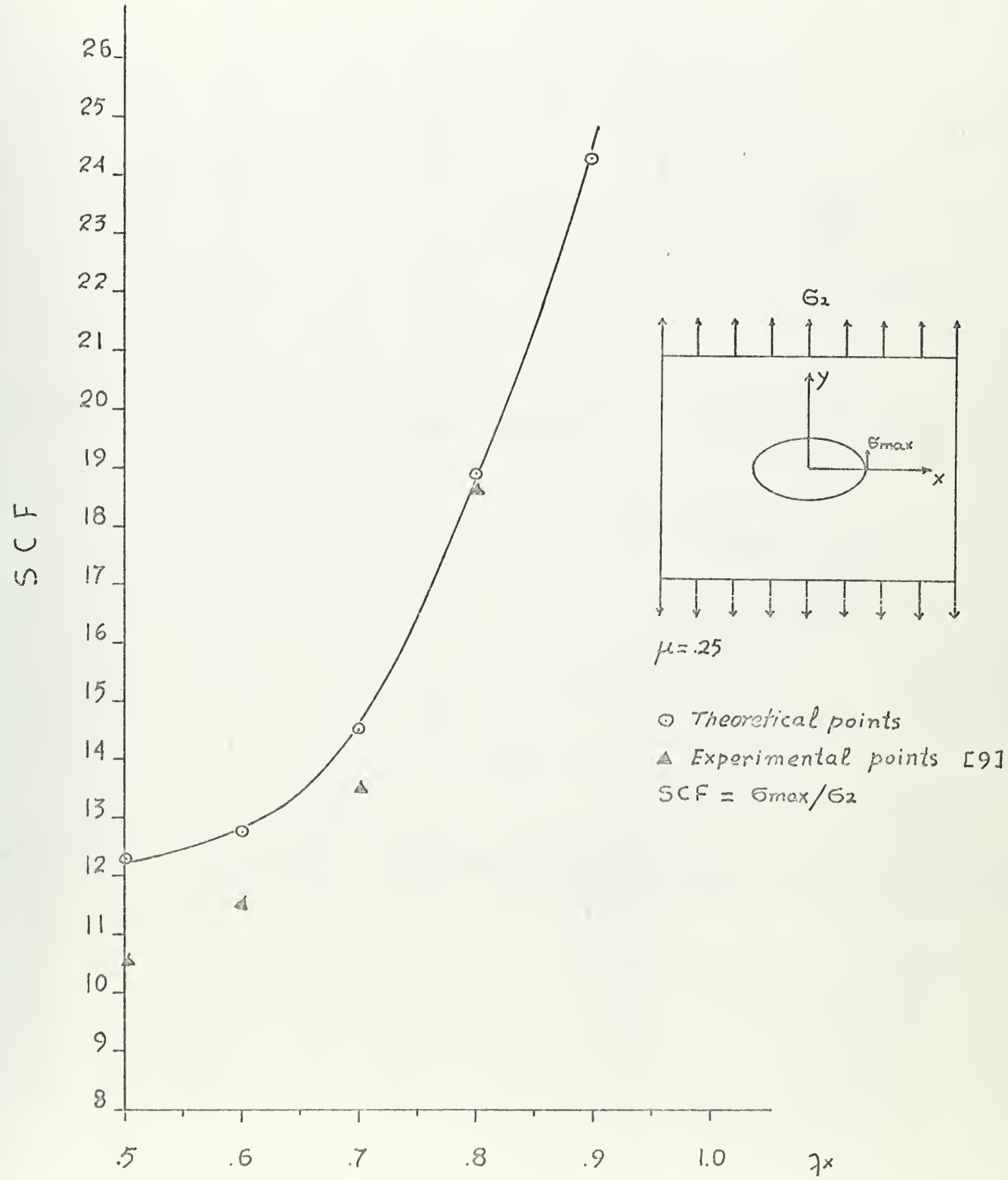
SCF
26
25
24
23
22
21
20
19
18
17
16
15
14
13
12
11
10
9
8
.5
.6
.7
.8
.9
1.0
λx
σ2
y
σmax
x
μ = .25
Theoretical points
Experimental points [9]
SCF = σmax/σ2

FIG 15

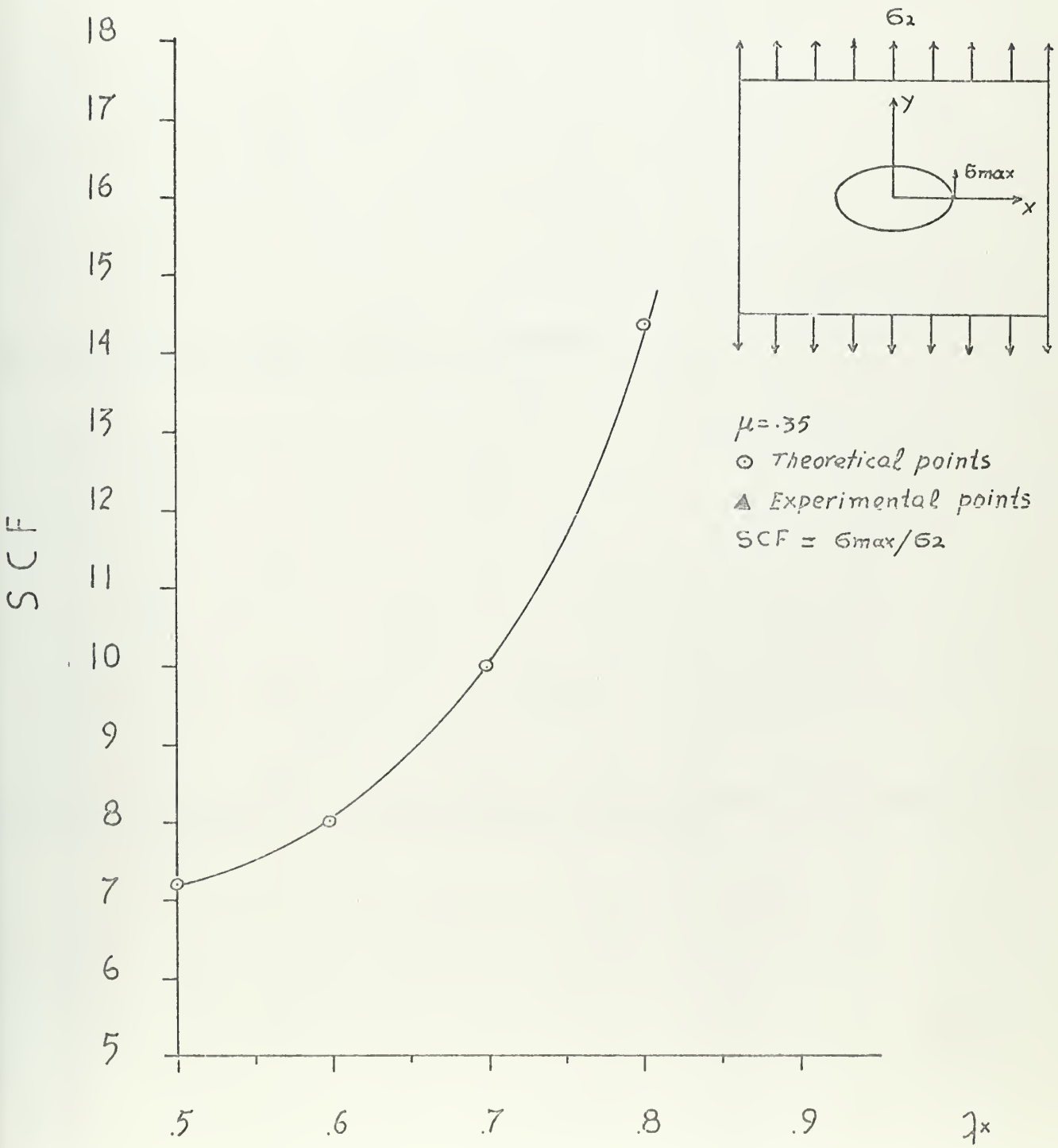
SCF
18
17
16
15
14
13
12
11
10
9
8
7
6
5
.5
.6
.7
.8
.9
η_x
σ_2
y
σ_{max}
x
$\mu = .35$
⊙ Theoretical points
▲ Experimental points
$SCF = \sigma_{max}/\sigma_2$

FIG 16

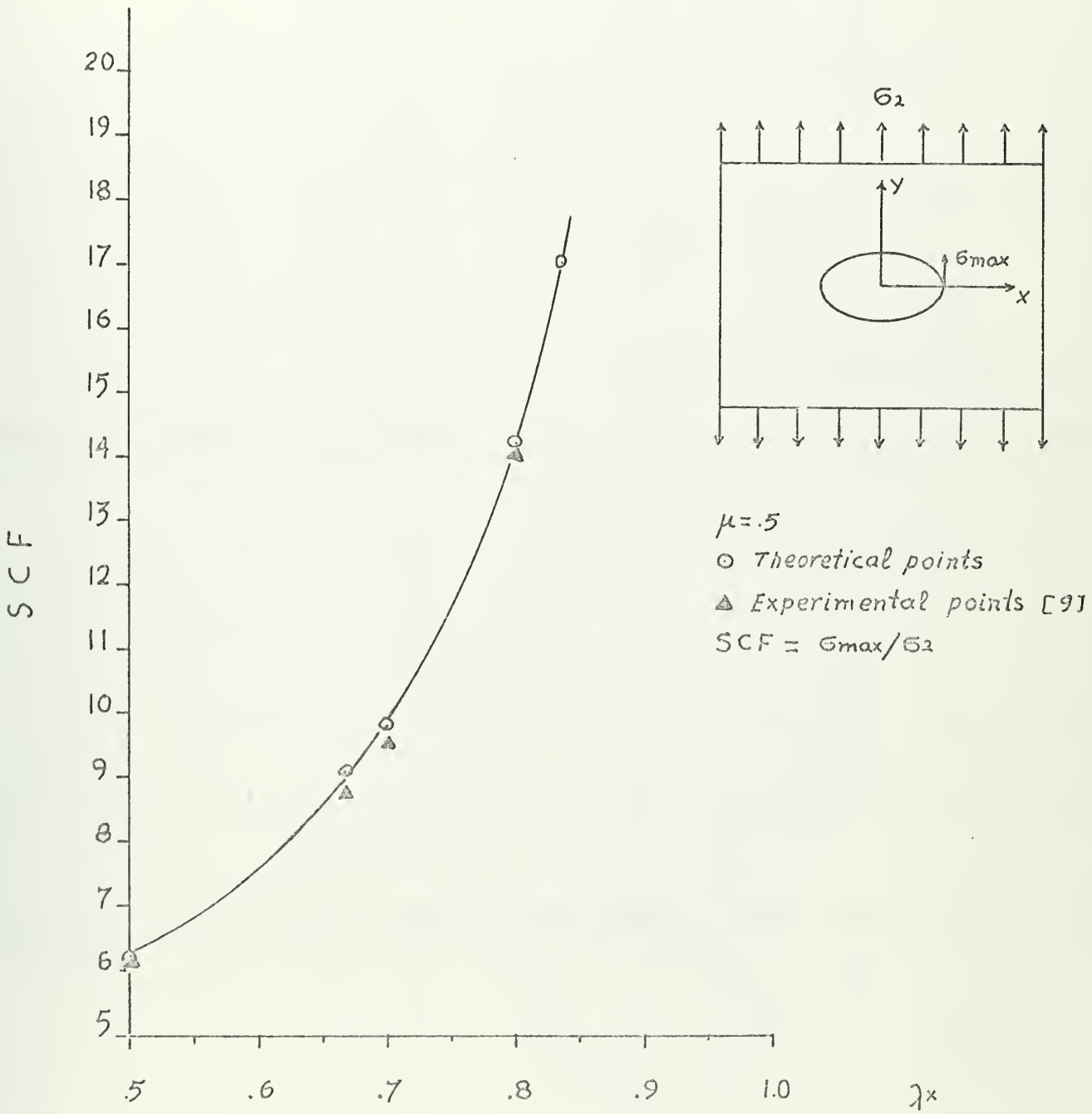
SCF
20
19
18
17
16
15
14
13
12
11
10
9
8
7
6
5
.5
.6
.7
.8
.9
1.0
λx
σ2
y
σmax
x
μ=.5
⊙ Theoretical points
△ Experimental points [9]
SCF = σmax/σ2

FIG 17

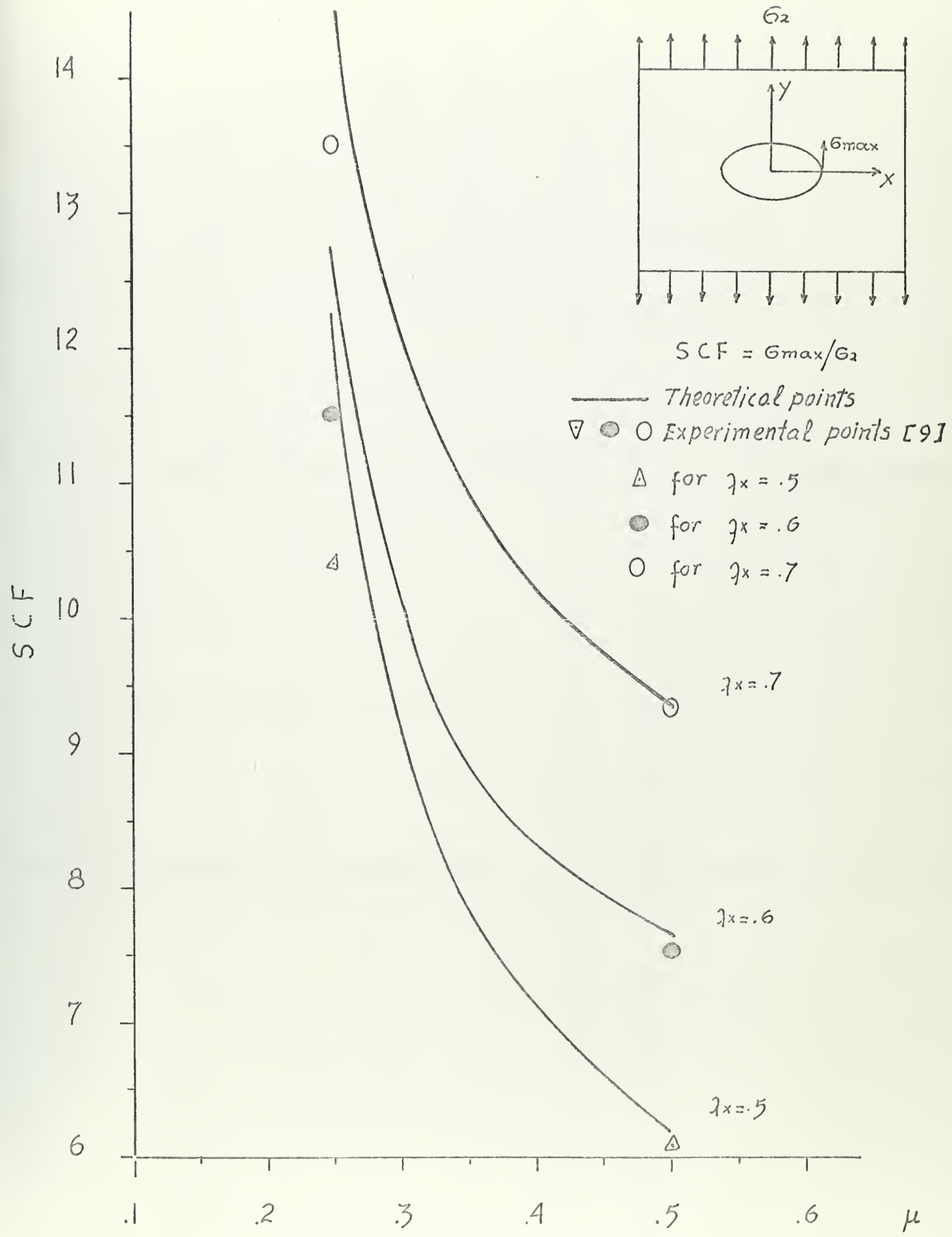
σ2
Y
σmax
X
SCF = σmax/σ2
Theoretical points
Experimental points [9]
for λx = .5
for λx = .6
for λx = .7
λx = .7
λx = .6
λx = .5
SCF
14
13
12
11
10
9
8
7
6
.1
.2
.3
.4
.5
.6
μ

FIG 18

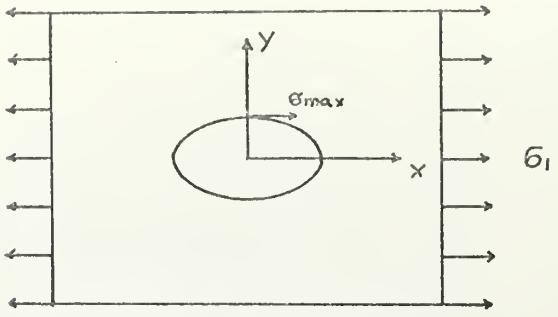
y
σmax
x
σ1

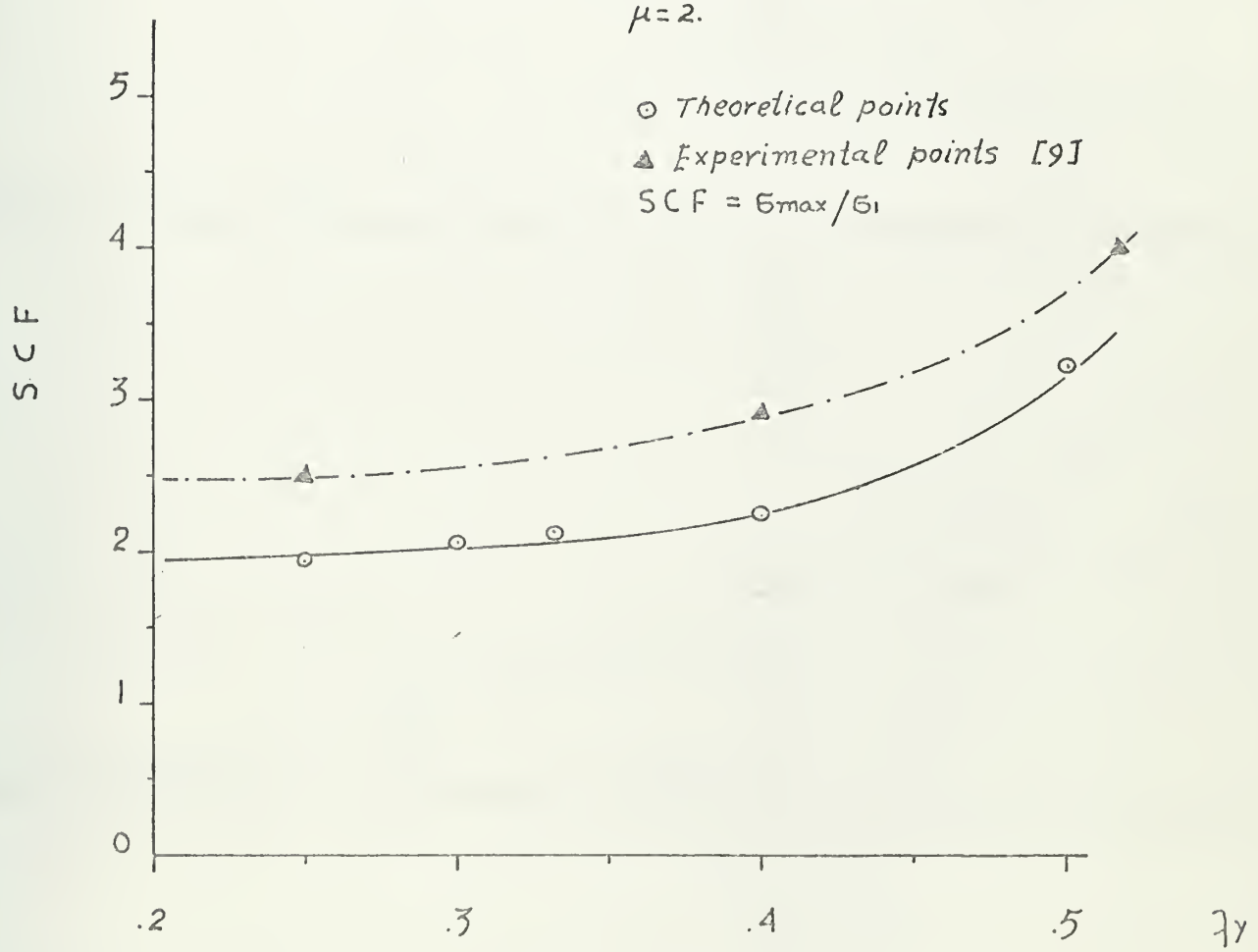
μ=2.
⊙ Theoretical points
▲ Experimental points [9]
SCF = σmax/σ1
SCF
5
4
3
2
1
0
.2
.3
.4
.5
γy

FIG 19

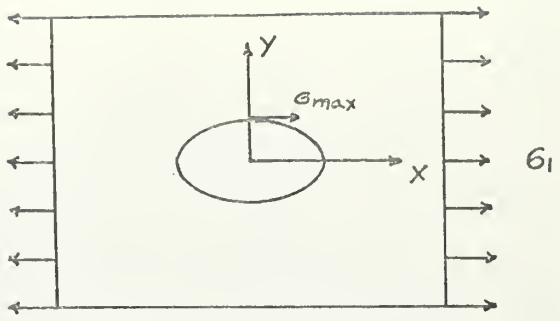

$SCF = \sigma_{max}/\sigma_1$

⊙ ▼ Theoretical points for $\mu = 2.5$, $\mu = 3$.

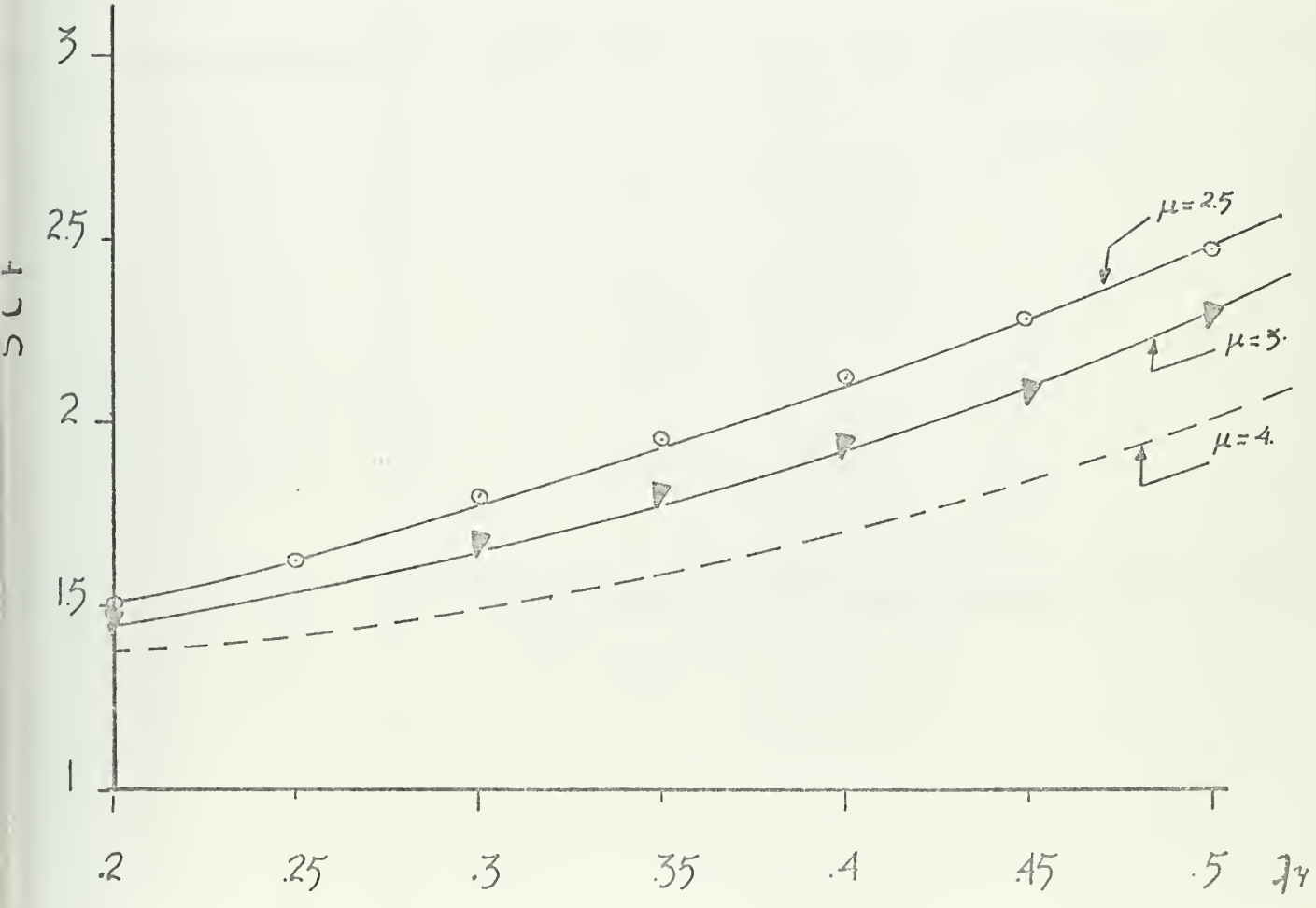

FIG 20

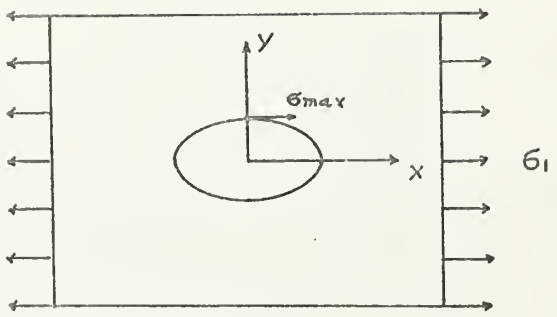

$\mu = 4.$

⊙ Theoretical points

▲ Experimental points [9]

SCF = σ_{max}/σ_1

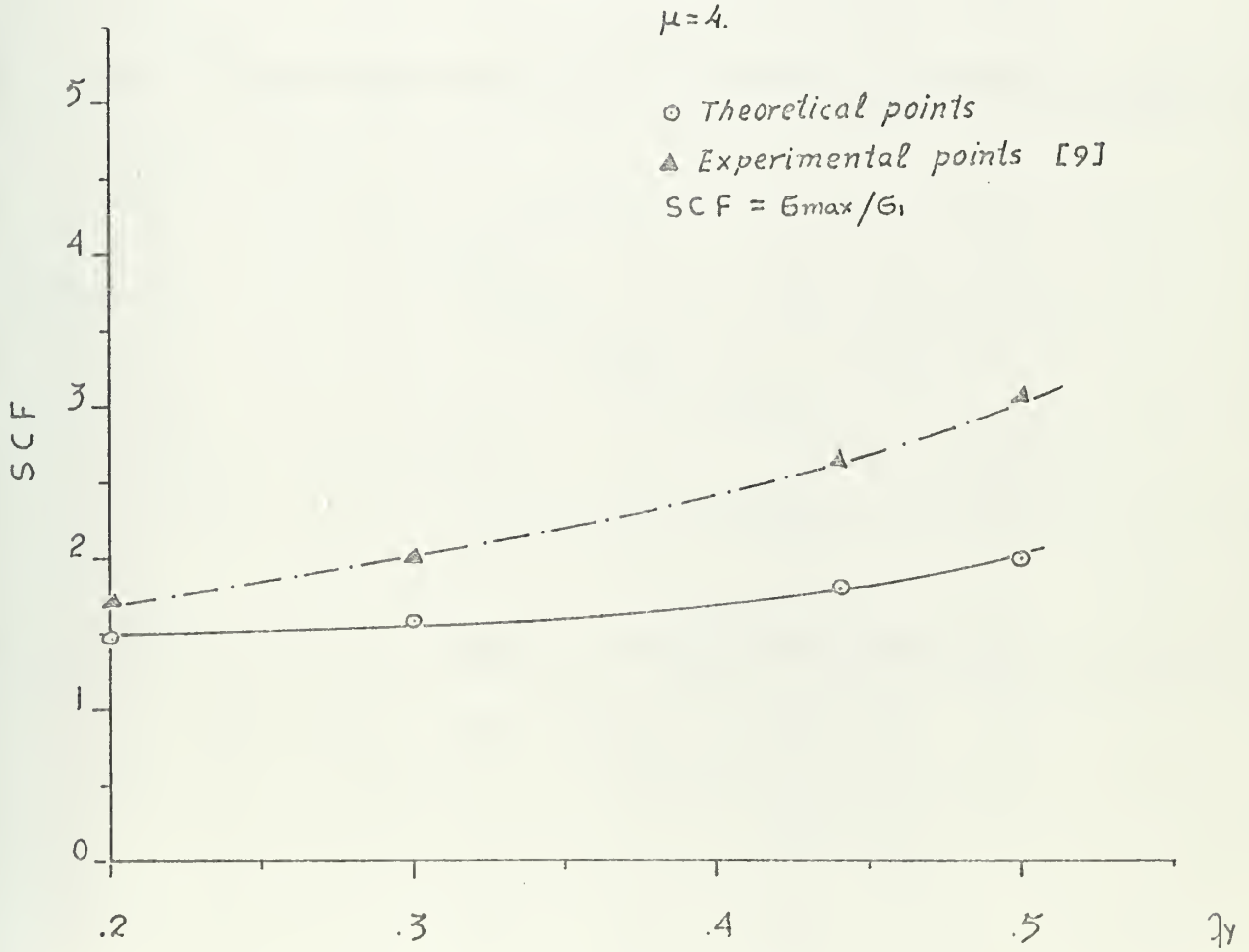

FIG 21

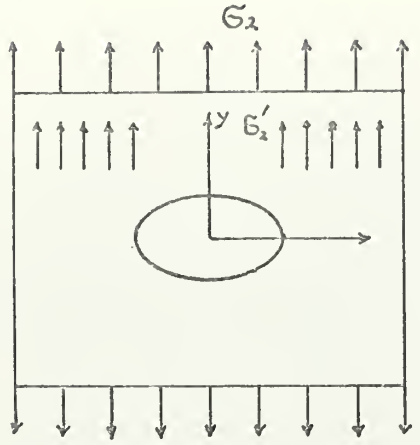

— Theoretical points

▲ Experimental points [9]

$\sigma_2' = \sigma_2/(1.-\gamma_x)$

$SCF' = \sigma_{max}/\sigma_2'$ for $\mu < 1.$

$\sigma_1' = \sigma_1/(1.-\gamma_y)$

$SCF' = \sigma_{max}/\sigma_1'$ for $\mu > 1.$

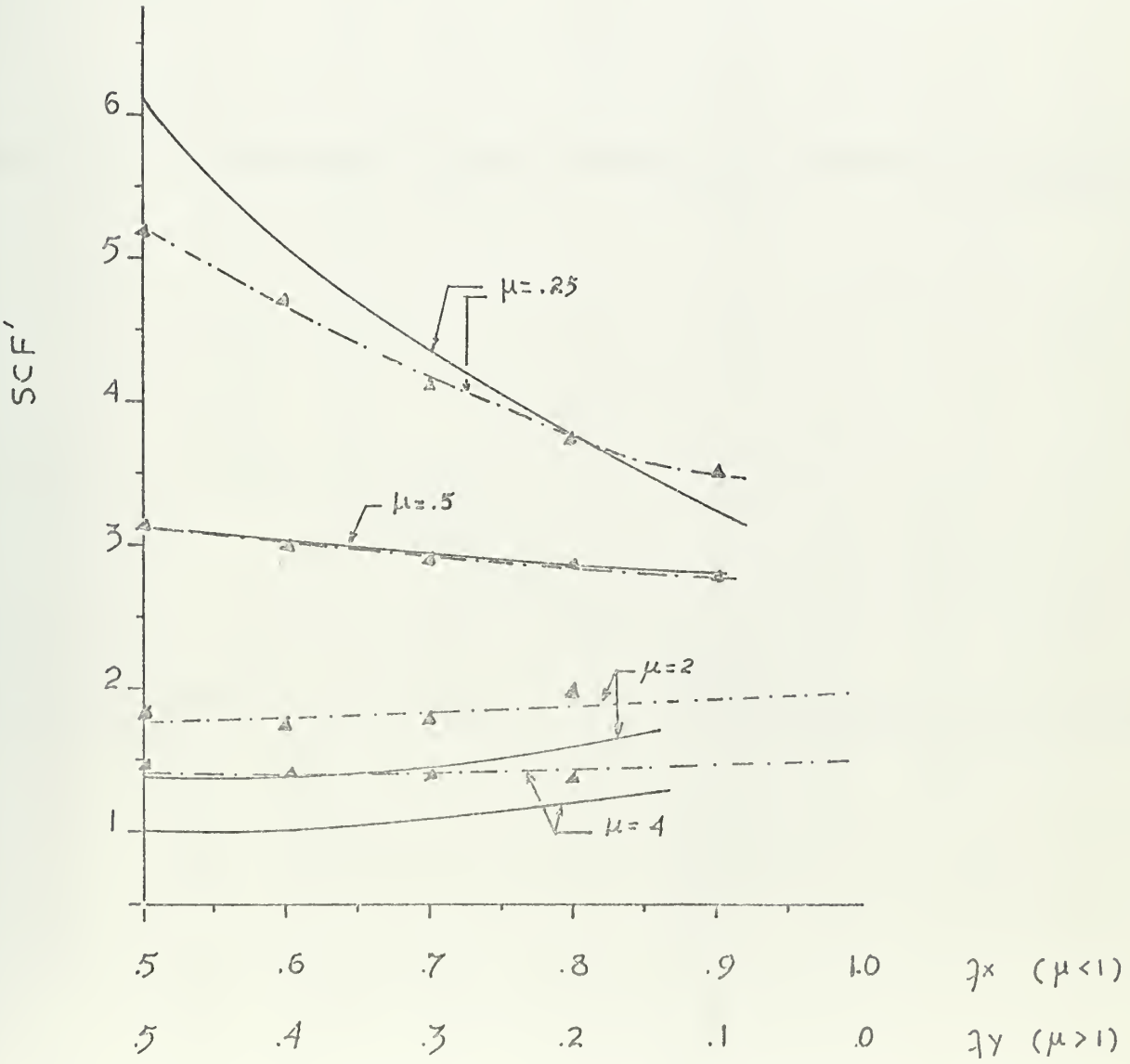

FIG 22

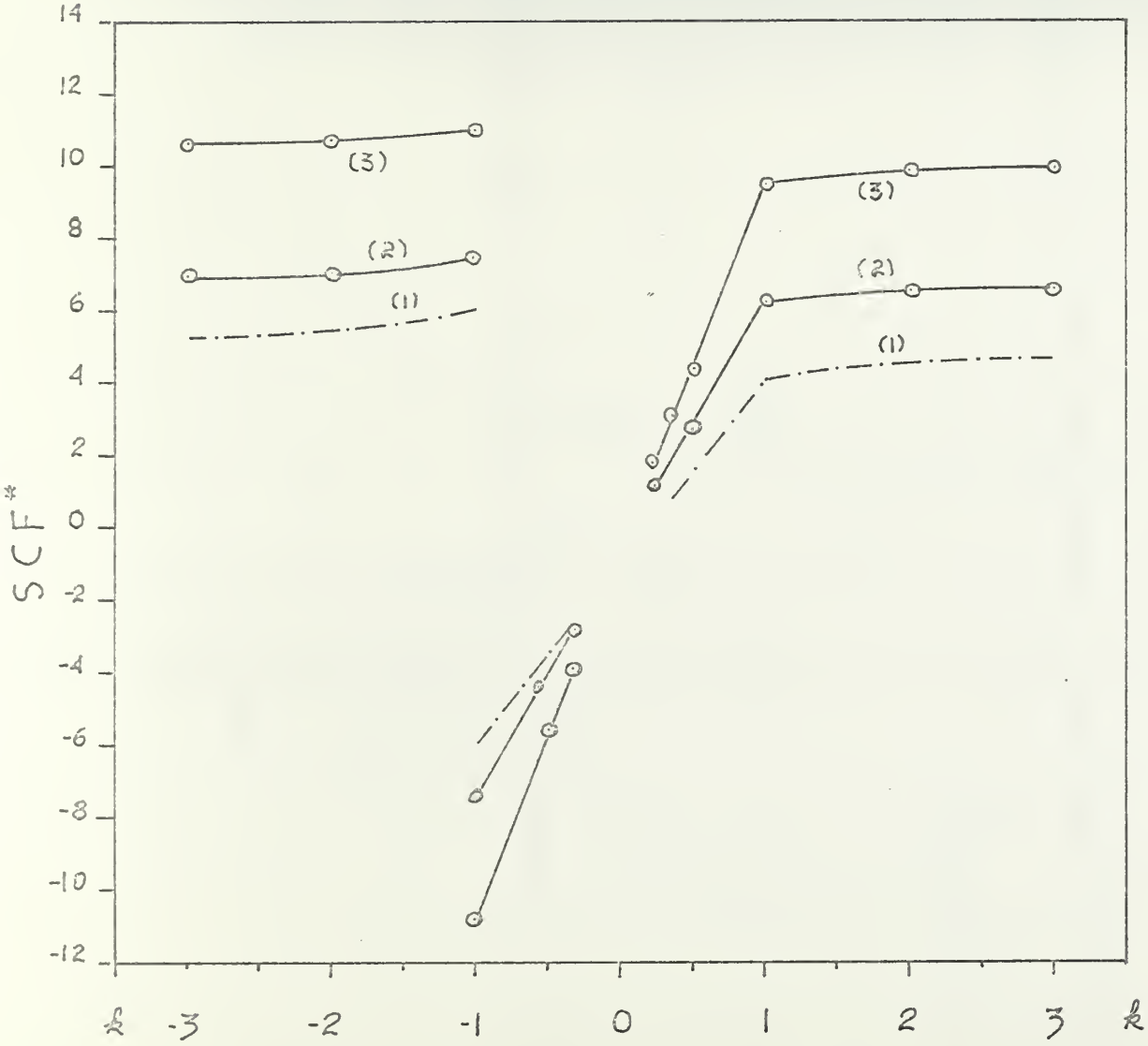

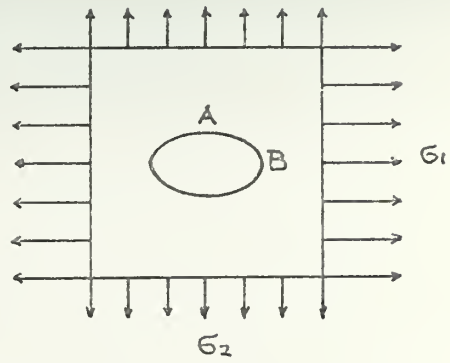

(1) Reproduced from [10]
$\mu = .5$; $\eta_x = .174$; $\eta_y = .087$

(2) Calculated
$\mu = .5$; $\eta_x = .5$; $\eta_y = .25$

(3) Calculated
$\mu = .5$; $\eta_x = .7$; $\eta_y = .35$

$k = \sigma_2/\sigma_1$

σ_{max} = Largest of $|\sigma_A|$ and $|\sigma_B|$

σ = Largest of $|\sigma_1|$ and $|\sigma_2|$

$SCF^* = \sigma_{max}/\sigma$

FIG 23

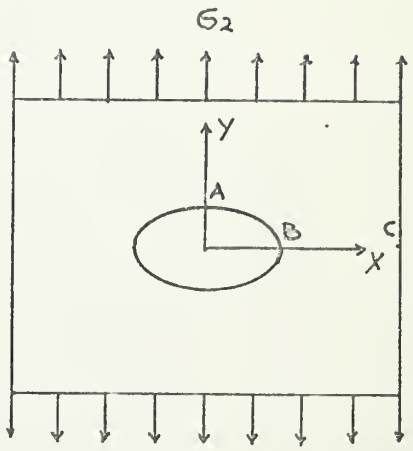

$\mu = .25$; $\eta_x = .8$

⊙ Theoretical points

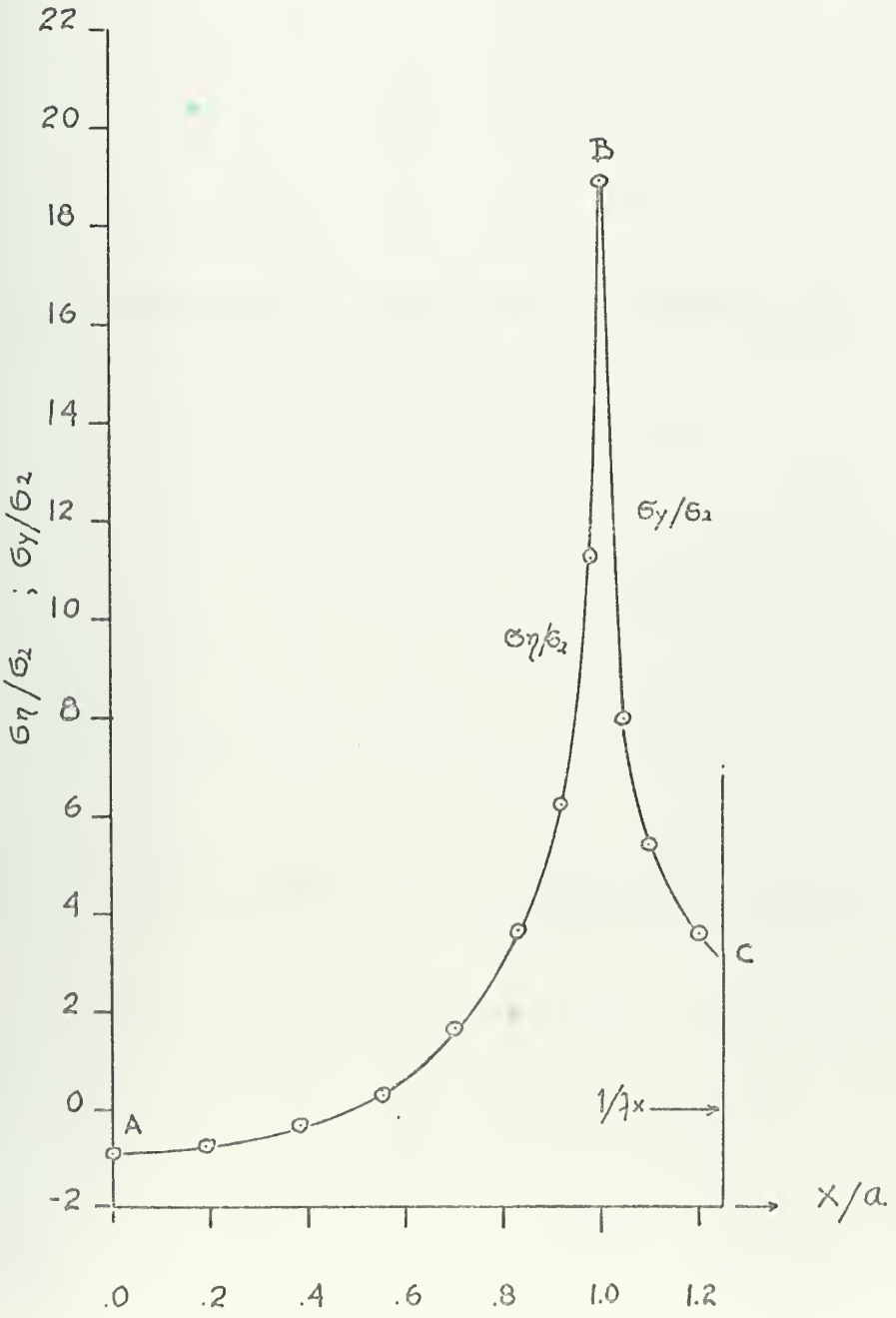

FIG 24

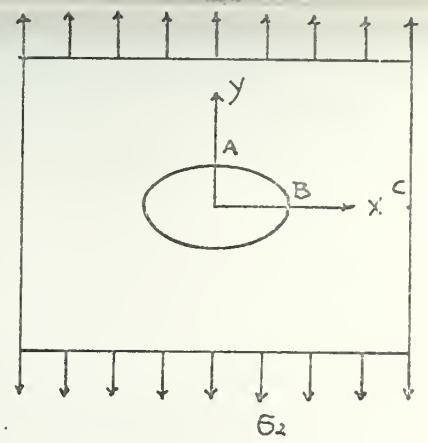

$\mu = .35$; $\gamma_x = .6$

⊙ Theoretical points

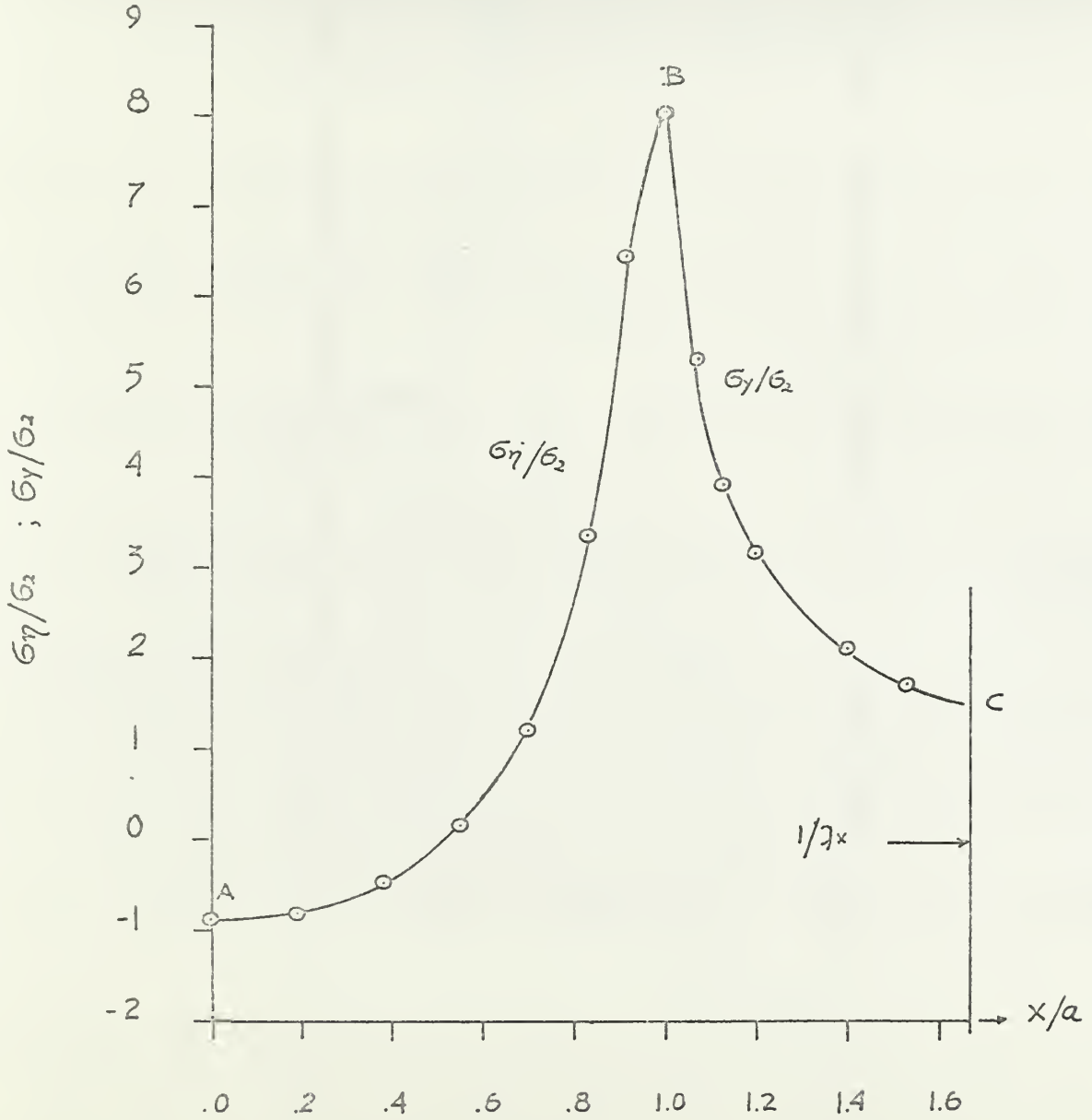

FIG 25

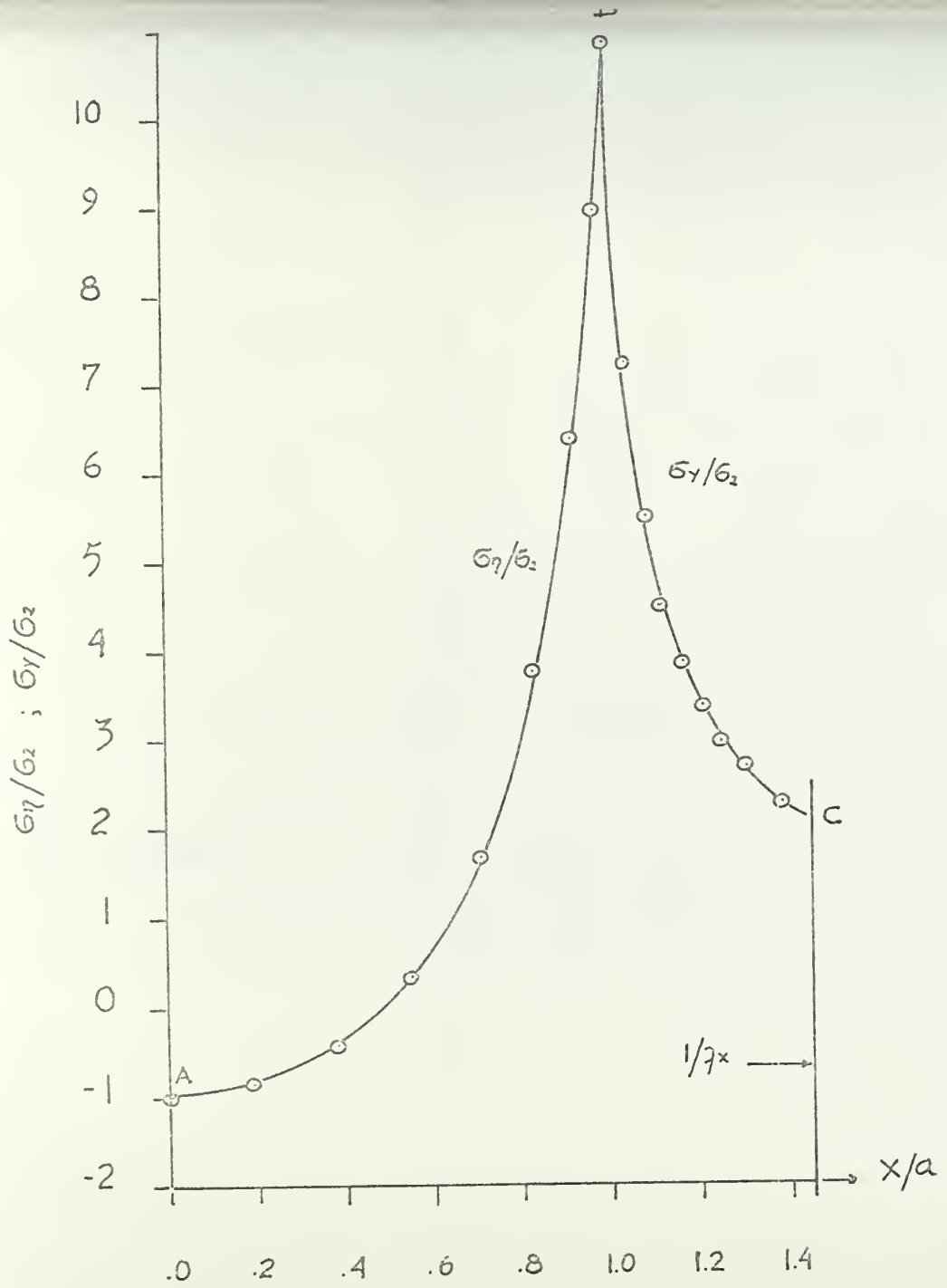

FIG 26

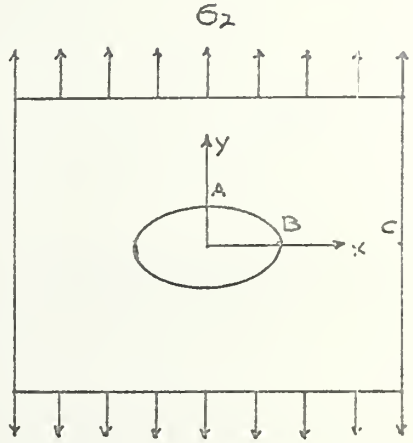

$\mu = .35$; $\gamma_x = .7$

⊙ Theoretical points

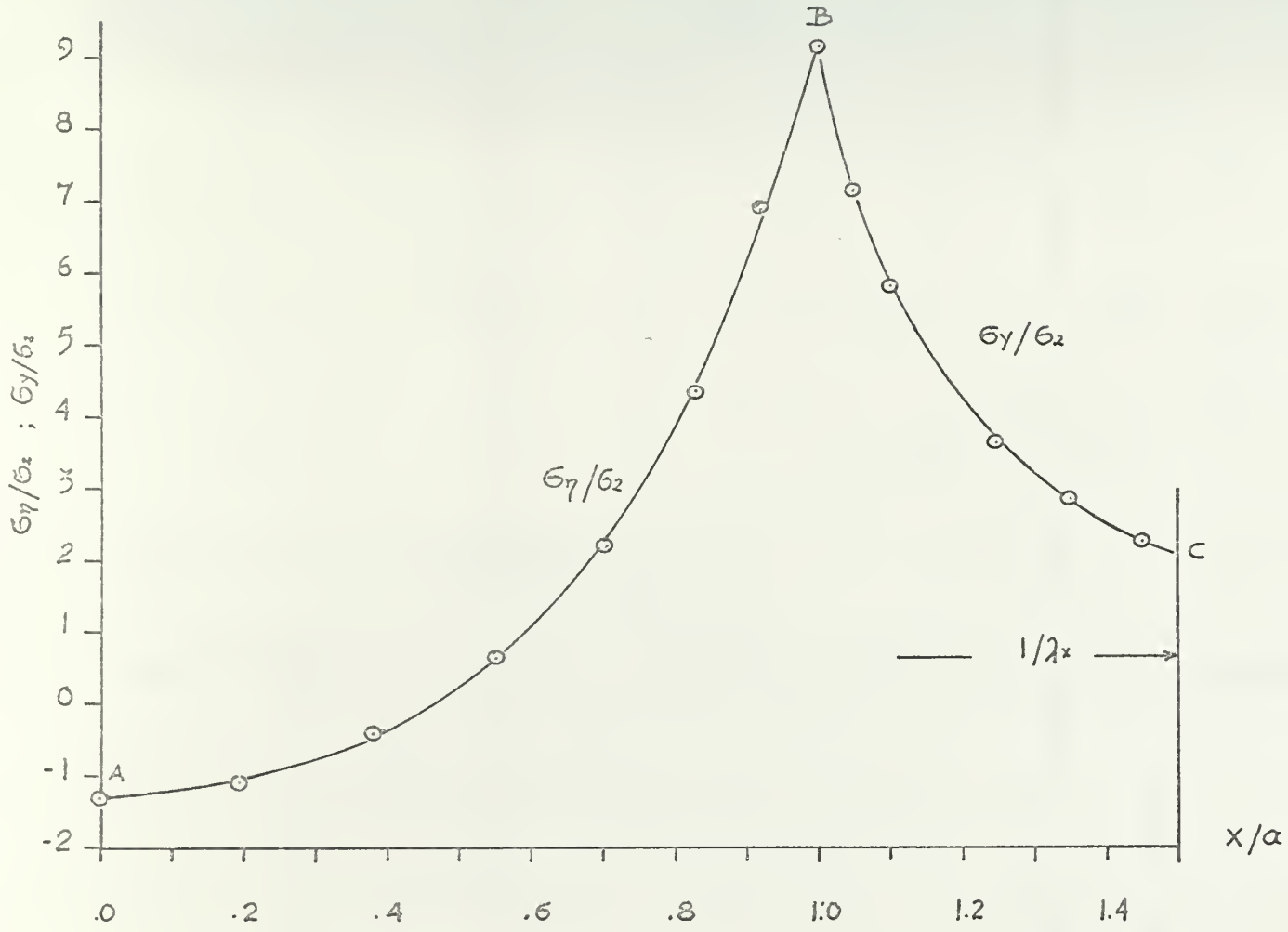

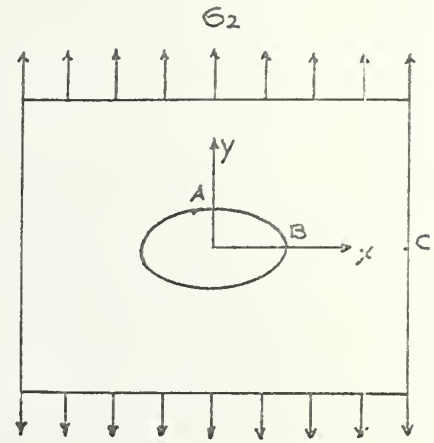

$\mu = .5$; $\lambda_x = .66$

⊙ Theoretical points

FIG 27

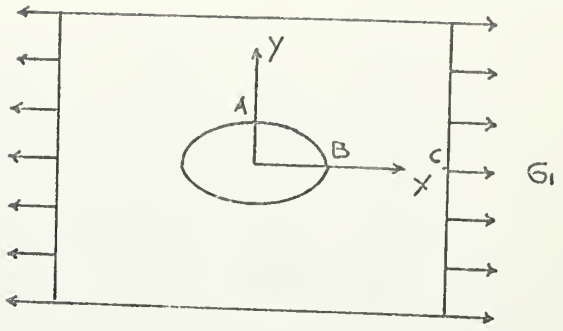

$\mu = 2.5$; $\gamma_y = .45$

⊙ Theoretical points

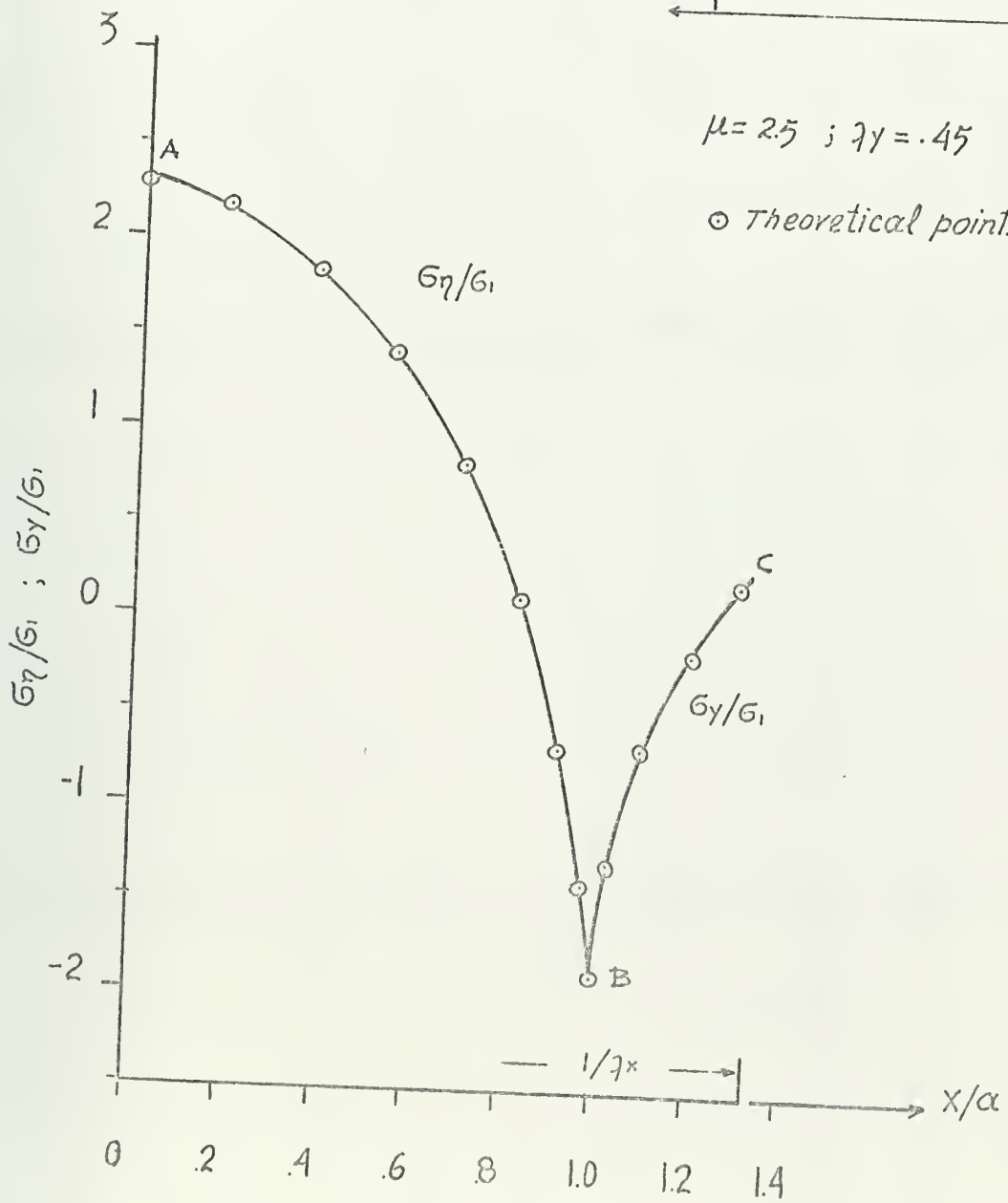

FIG 28

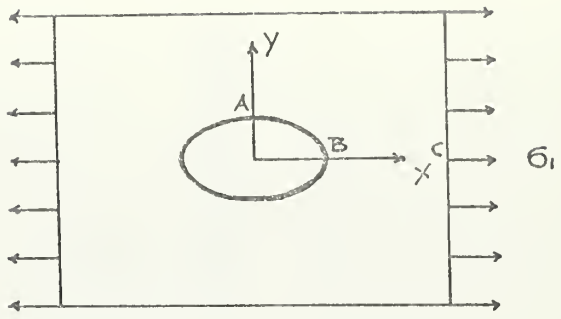
y
A
B
C
x
σ1

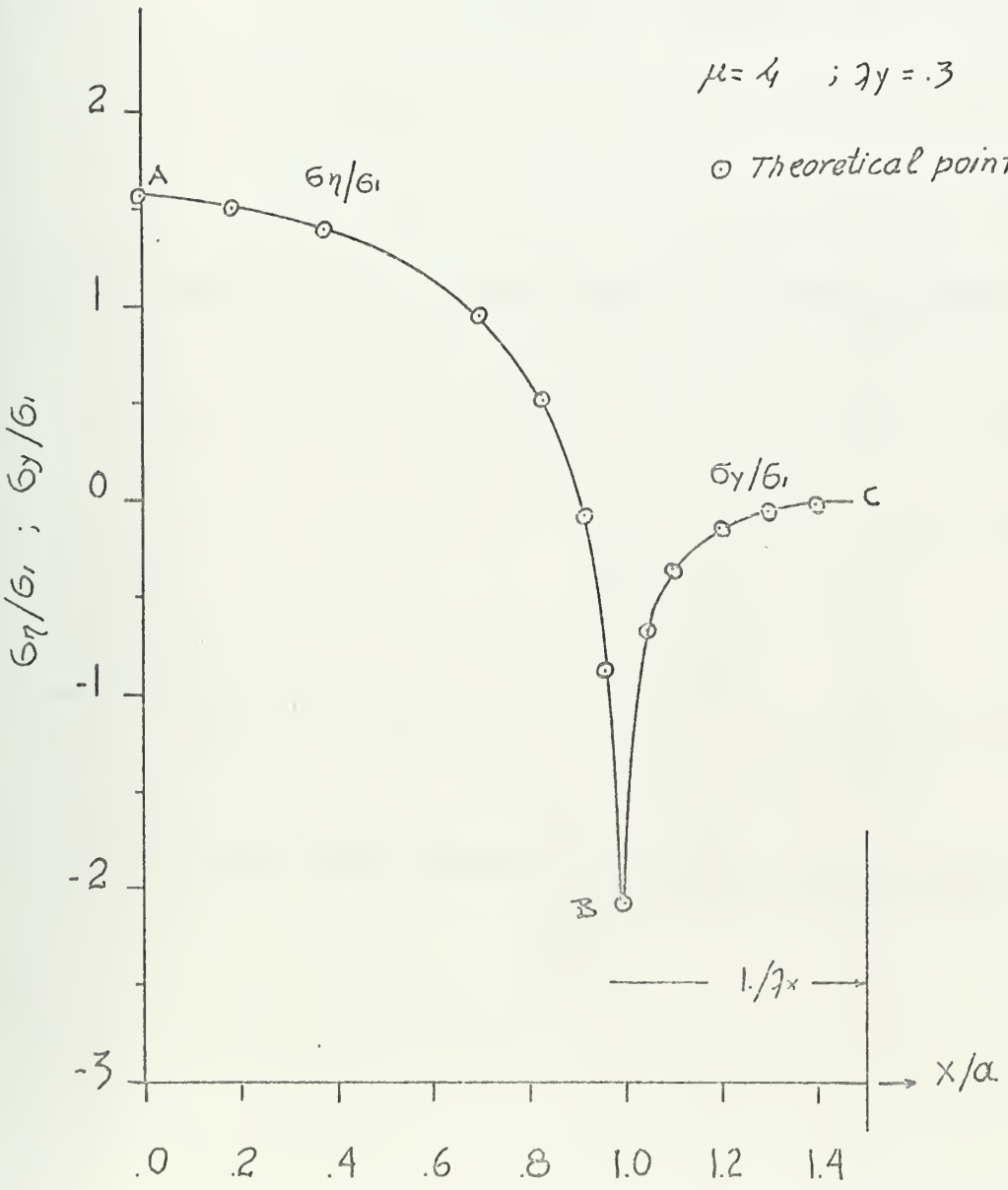
μ = 4 ; γy = .3
⊙ Theoretical points
ση/σ1
σy/σ1
A
B
C
ση/σ1 ; σy/σ1
2
1
0
-1
-2
-3
1./γx
x/a
.0
.2
.4
.6
.8
1.0
1.2
1.4

FIG 29

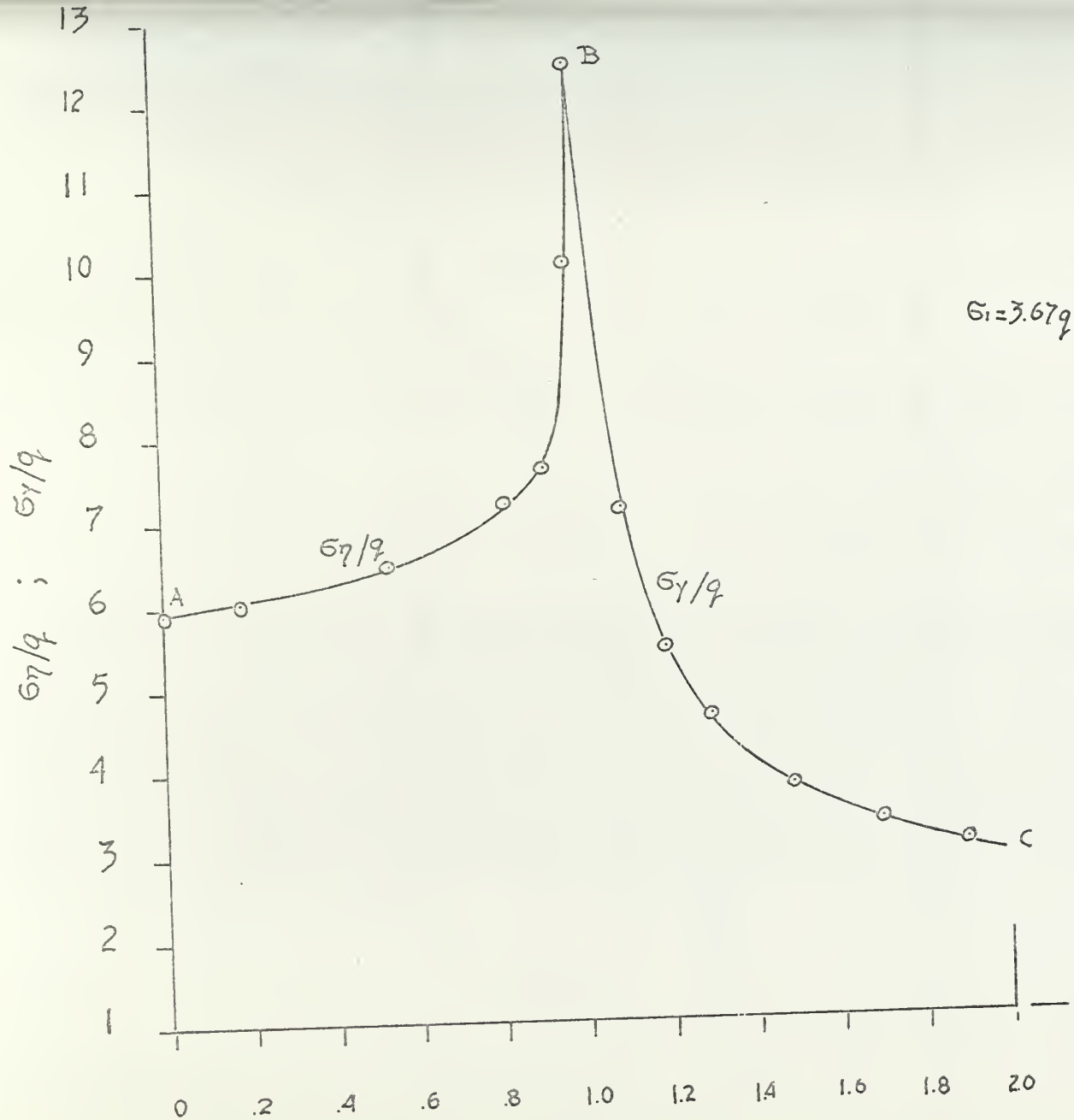

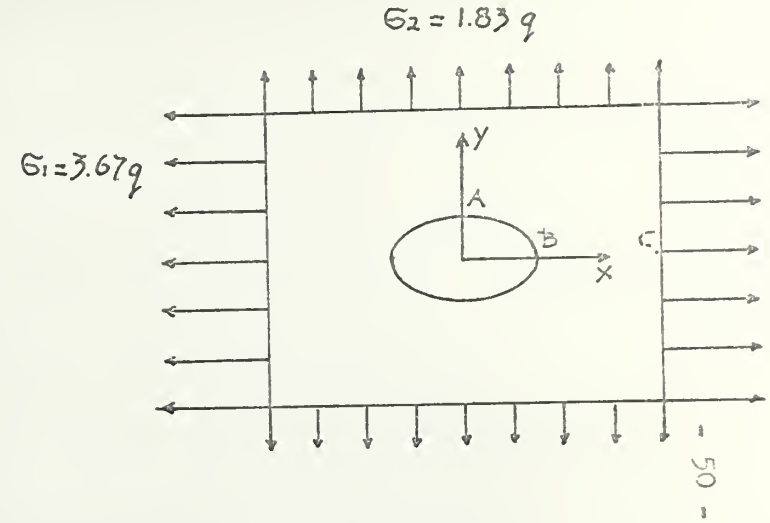

$\mu = .5$

$\gamma_x = .5$

$\gamma_y = .25$

⊙ Theoretical points

q = Unit load

FIG 30

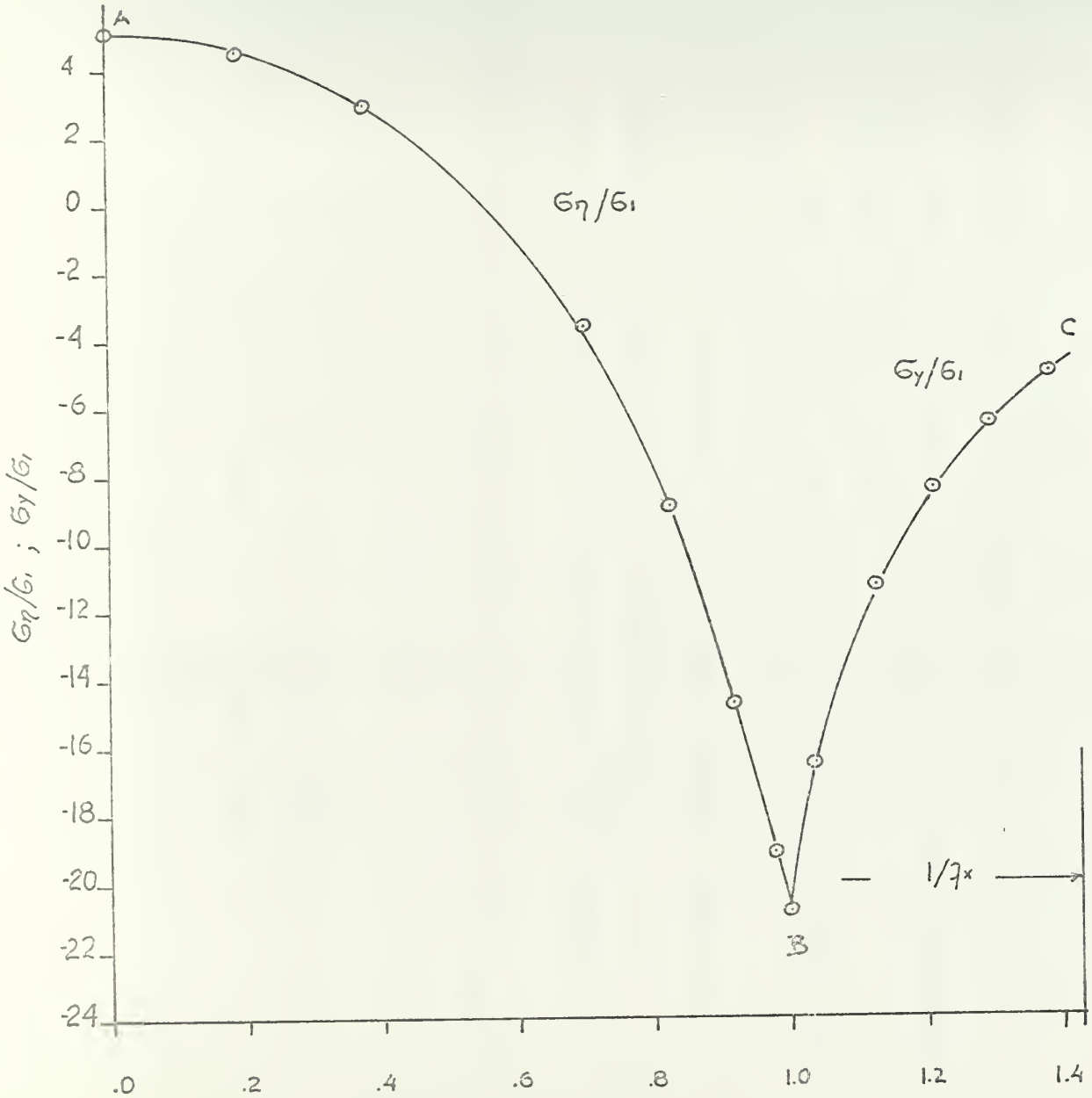

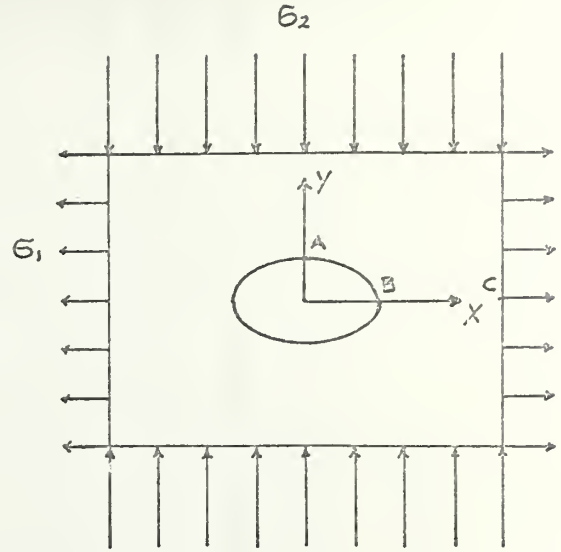

$\mu = .5$

$\gamma_x = .7$

$\gamma_y = .35$

⊙ Theoretical points

$\sigma_2 = -2\sigma_1$

FIG 31

RESULTS

Figures 3 up to 31 are typical plots of results obtained from the computer program. Whenever possible, experimental data are indicated. Most of the figures are selfexplanatory but additional information, if necessary, is given in the discussion of each figure.

Figures 3 up to 14 show the stress distribution around the boundary of the elliptical hole in finite plates for several values of μ and γ.

It should be noted that in cases of loading parallel to the minor axis, the tensile stresses predicted are 2% to 17% higher than experiments reported in [9] while the much smaller compressive stresses are 40% to 60% lower.

When the external loading is parallel to the major axis of the ellipse the agreement with [9] lies between 5% and 25%.

The above differences in compressive stresses, when loading parallel to the major axis are of minor importance from an engineering point of view because, these stresses are very small compared to the maximum tensile ones.

Figures 15 up to 22 show the maximum tensile stresses (SCF and SCF') as function of γ for several values of μ . (Finite plate with one elliptical hole).

In figure 23 several cases of biaxial loading are plotted. It was not possible to examine the same plate used in [10] because of γ limitations discussed previously. Other plates were examined

and the definitions from [10] were used.

The curves appear to have the same shape.

Figures 24 up to 31 show the σ_η and σ_y distribution around the boundary of the elliptical hole and the x axis respectively for typical uniaxial and biaxial loading.

CONCLUSIONS

The stress functions assumed have been shown to give results that are comparable with available experimental data and therefore some confidence exists in the theoretical predictions for cases where no experimental results exist.

The stress concentration factors for plates perforated with elliptical holes under in-plane loading, appear to be much higher in comparison with similar plates perforated with circular holes.

Certain disagreements have been noticed between measured and predicted stresses in the low level compressive stress range, while the predictions for the high level tensile stresses are somewhat higher than the measured ones but still in close agreement.

RECOMMENDATIONS

The following topics are recommended for further investigation:

a.- Postulation of similar stress functions in terms of hyperbolic functions instead of positive exponentials, in association with other functions decaying rapidly as increases in order to be more suitable for computer use. Timpe in [13] suggests such stress functions.

b.- Study of the problem for cases of loading that produce antisymmetrical conditions (shear forces applied on the edges of the plate for example), will be rather easy to handle.

APPENDIX 1

Equations (11), (12) and (13) may be rearranged in the form of (24), (25) and (26), respectively. Also equations (14), (15) and (16) are rearranged in the form of (27), (28) and (29) respectively.

$$\sigma_\xi \frac{4J^4}{c^2} = \sum_{n=1,3\ldots}^{\infty} C_n\, n \Big\{ e^{(n-1)\xi} \big[(n+1)\cos(n+3)\eta + 4\cos(n-1)\eta\big] +$$

$$+ e^{(n+1)\xi} \big[-4\cos(n+1)\eta + (n-1)\cos(n-3)\eta\big] +$$

$$+ e^{(n-3)\xi} \big[-(n+3)\cos(n+1)\eta\big] +$$

$$+ e^{(n+3)\xi} \big[-(n-3)\cos(n-1)\eta\big]\Big\}$$

$$+ \sum_{n=1,3\ldots}^{\infty} D_n\, n \Big\{ e^{-(n-1)\xi} \big[(n+1)\cos(n+3)\eta + 4\cos(n-1)\eta\big] +$$

$$+ e^{-(n+1)\xi} \big[-4\cos(n+1)\eta + (n-1)\cos(n-3)\eta\big] +$$

$$+ e^{-(n-3)\xi} \big[-(n+3)\cos(n+1)\eta\big] +$$

$$+ e^{-(n+3)\xi} \big[-(n-3)\cos(n-1)\eta\big]\Big\}$$

$$+ \sum_{n=2,4\ldots}^{\infty} G_\eta\, n \Big\{ e^{(n-2)\xi} \big[-(n+1)\cos n\eta\big] + e^{n\xi} \big[(n-1)\cos(n+2)\eta +$$

$$+ (n+1)\cos(n-2)\eta\big] +$$

$$+ e^{(n+2)\xi}\left[-(n-1)\cos n\eta\right]\Big\} +$$

$$H_n\, n\Big\{e^{-(n-2)\xi}\left[-(n+1)\cos n\eta\right] + e^{-n\xi}\left[(n-1)\cos(n+2)\eta + \right.$$

$$\left. + (n+1)\cos(n-2)\eta\right] + e^{-(n+2)\xi}\left[-(n-1)\cos n\eta\right]\Big\} +$$

$$+ 2A_0 \sin 2\xi \qquad (24)$$

$$\sigma_\eta \frac{4J^4}{c^2} = \sum_{n=1,3\ldots}^{\infty} C_n\, n\Big\{e^{(n-3)\xi}\left[(n-1)\cos(n+1)\eta\right] + e^{(n-1)\xi}\left[-(n-3)\cos(n+3)\eta + \right.$$

$$\left. + 4\cos(n-1)\eta\right] + e^{(n+1)\xi}\left[-4\cos(n+1)\eta - \right.$$

$$\left. - (n+3)\cos(n-3)\eta\right] + e^{(n+3)\xi}\left[(n+1)\cos(n-1)\eta\right]\Big\}$$

$$+\sum_{n=1,3\ldots}^{\infty} D_n\, n\Big\{e^{-(n-3)}\left[(n-1)\cos(n+1)\eta\right] + e^{-(n-1)\xi}\left[-(n-3)\cos(n+3)\eta + \right.$$

$$\left. + 4\cos(n-1)\eta\right] + e^{-(n+1)\xi}\left[-4\cos(n+1)\eta - \right.$$

$$\left. - (n+3)\cos(n-3)\eta\right] + e^{-(n+3)\xi}\left[(n+1)\cos(n-1)\eta\right]\Big\}$$

$$+\sum_{n=2,4\ldots}^{\infty} G_n\, n\Big\{e^{(n-2)\xi}\left[(n+1)\cos n\eta\right] + e^{n\xi}\left[-(n-1)\cos(n+2)\eta - \right.$$

$$\left. - (n+1)\cos(n-2)\eta\right] + e^{(n+2)\xi}\left[(n-1)\cos n\eta\right]\Big\} +$$

$$+\sum_{n=2,4\ldots}^{\infty} H_n\, n\Big\{e^{-(n-2)\xi}\left[(n+1)\cos n\eta\right] + e^{-n\xi}\left[-(n-1)\cos(n+2)\eta - \right.$$

$$-(n+1)\cos(n-2)\eta\Big] + e^{-(n+2)\xi}\Big[(n-1)\cos n\eta\Big]\Big\} +$$

$$+ A_o\left(-2\sinh 2\xi\right) \qquad (25)$$

$$\tau_{\xi n}\frac{4J^4}{c^2} = \sum_{n=1,3\ldots}^{\infty} C_n n\Big\{e^{(n-3)\xi}\Big[(n+1)\sin(n+1)\eta\Big] - e^{(n-1)\xi}\Big[\sin(n+3)\eta\Big] -$$

$$- e^{(n+1)\xi}(n+1)\sin(n-3)\eta + e^{(n+3)\xi}(n-1)\sin(n-1)\eta\Big\} +$$

$$+ \sum_{n=1,3\ldots}^{\infty} D_n n\Big\{-e^{-(n-3)}(n+1)\sin(n+1)\eta + e^{-(n-1)\xi}\sin(n+3)\eta +$$

$$+ e^{-(n+1)\xi}(n+1)\sin(n-3)\eta - e^{-(n+3)\xi}(n-1)\sin(n-1)\eta\Big\} +$$

$$+ \sum_{n=2,4\ldots}^{\infty} G_n n\Big\{e^{(n-2)\xi}(n+1)\sin n\eta - e^{n\xi}(n+1)\sin(n-2)\eta +$$

$$+ (n-1)\sin(n+2)\eta + e^{(n+2)\xi}(n-1)\sin n\eta\Big\} +$$

$$+ \sum_{n=2,4\ldots}^{\infty} H_n n\Big\{-e^{-(n-2)\xi}(n+1)\sin n\eta + e^{-n\xi}(n+1)\sin(n-2)\eta +$$

$$+ (n-1)\sin(n+2)\eta + e^{-(n+2)\xi}(-n+1)\sin n\eta\Big\} +$$

$$+ A_o\, 2\sin 2\eta \qquad (26)$$

$$\sigma_x\frac{4J^4}{c^2} = \sum_{n=1,3\ldots}^{\infty} C_n\Big[\sin^2\alpha\, A_{in} + \cos^2\alpha\, B_{in} - \sin 2\alpha\, AB_{in}\Big] +$$

$$+ \sum_{n=1,3\ldots}^{\infty} D_n \left[\sin^2\alpha\, A_{2n} + \cos^2\alpha\, B_{2n} - \sin 2\alpha\, AB_{2n}\right] +$$

$$+ \sum_{n=2,4\ldots}^{\infty} G_n \left[\sin^2\alpha\, A_{3n} + \cos^2\alpha\, B_{3n} - \sin 2\alpha\, AB_{3n}\right] +$$

$$+ \sum_{n=2,4\ldots}^{\infty} H_n \left[\sin^2\alpha\, A_{4n} + \cos^2\alpha\, B_{4n} - \sin 2\alpha\, AB_{4n}\right] +$$

$$+ A_o \left[-2\sin 2\xi \cos 2\alpha - 2\sin 2\alpha \sin 2\eta\right] \qquad (27)$$

$$\sigma_y \frac{4J^4}{c^2} = \sum_{n=1,3\ldots}^{\infty} C_n \left[\cos^2\alpha\, A_{1n} + \sin^2\alpha\, B_{1n} + \sin 2\alpha\, AB_{1n}\right] +$$

$$+ \sum_{n=1,3\ldots}^{\infty} D_n \left[\cos^2\alpha\, A_{2n} + \sin^2\alpha\, B_{2n} + \sin 2\alpha\, AB_{2n}\right] +$$

$$+ \sum_{n=2,4\ldots}^{\infty} G_n \left[\cos^2\alpha\, A_{3n} + \sin^2\alpha\, B_{3n} + \sin 2\alpha\, AB_{3n}\right] +$$

$$+ \sum_{n=2,4\ldots}^{\infty} H_n \left[\cos^2\alpha\, A_{4n} + \sin^2\alpha\, B_{4n} + \sin 2\alpha\, AB_{4n}\right] +$$

$$+ A_o \left[2\cos^2\alpha \sinh 2\xi - 2\sin^2\alpha \sin 2\xi + \right.$$

$$\left. + 2\sin 2\alpha \sin 2\eta\right] \qquad (28)$$

$$\tau_{xy} \frac{4J^4}{c^2} = \sum_{n=1,3\ldots}^{\infty} C_n \left[\frac{1}{2}(A_{1n} - B_{1n})\sin 2\alpha - AB_{1n}\cos 2\alpha\right] +$$

$$+ \sum_{n=1,3\ldots}^{\infty} D_n \left[\frac{1}{2}(A_{2n} - B_{2n})\sin 2\alpha - AB_{2n}\cos 2\alpha\right] +$$

$$+\sum_{n=2,4\ldots}^{\infty} Gn\left[\frac{1}{2}\left(A_{3n}-B_{3n}\right)\sin 2\alpha - AB_{3n}\cos 2\alpha\right] +$$

$$+\sum_{n=2,4\ldots}^{\infty} Hn\left[\frac{1}{2}\left(A_{4n}-B_{4n}\right)\sin 2\alpha - AB_{3n}\cos 2\alpha\right] +$$

$$+ A_0\left[\left(\sin 2\xi + \sinh 2\xi\right)\sin 2\alpha -\right.$$

$$\left. - 2\sin 2\eta\cos 2\alpha\right] \qquad (29)$$

In the above expressions for σ_x , σ_y , τ_{xy} :

Ain (i = 1, 2, 3, 4) represent the coefficients of Cn, Dn, Gn, Hn, respectively, from the expression for σ_ξ

Bin (i = 1, 2, 3, 4) represent the coefficients of Cn, Dn, Gn, Hn, respectively, from the expression for σ_η

ABin (i = 1, 2, 3, 4) represent the coefficients of Cn, Dn, Gn, Hn, respectively, from the expression for $\tau_{\xi\eta}$

The value of ξ is obtained by using the formula

$$\xi = \frac{1}{2}\log\left(\frac{1+b'/a'}{1-b'/a'}\right) \qquad (30)$$

It is obvious that as $\eta \to 0$ (i.e. $\alpha \ll W_x$) $b' \to a'$ and therefore $\xi \to \infty$.

Analyzing the case of figure 2d, for example, the use of equations (24) and (26) according to (19a) and (19b) generates a set of 12 equations, if six fixed points are selected on the boundary of the (quadrant) ellipse

Another set of six equations is generated by using (27) and (29) according to (21), if three points are selected on $x=3''$.

Finally six more equations are generated by using (28) and (29) according to (20), if another three points are selected on $y=3''$.

It should be noted that the number of unknown constants was selected to be 21.

The system obtained this way has 24 equations with 21 unknowns and it is solved by following the procedure described in section NUMERICAL METHOD.

The matrix A^T is formed and A and B are premultiplied by A^T and from the solution of the system

$$A^T A X = A^T B$$

we obtain the values of the unknown constants.

Summarizing the above procedure, we have chosen a number of points greater than the number of unknown constants and we required that the boundary conditions be satisfied as nearly as possible at

these points (Least square sense) Ref. [14].

Because of the nature of the assumed series solution, the number of unknown constants is always odd when truncating the series at any value of n. Therefore the system of equations is always overdetermined at least by one equation.

REFERENCES

1.- Timoshenko, S., and Goodier, J.N., "Theory of Elasticity" McGraw-Hill, 1951.

2.- Ling, C.B., "On the Stresses in a Plate Containing Two Circular Holes", Jnl. App. Phys., Vol.19, 1948.

3.- Peterson, R.E., "The Interaction Effect of Neighboring Holes or Cavities With Particular Reference to Pressure Vessels and Rocket Cases", Trans. A.S.M.E., Jnl. Basic Eng., Dec. 1965.

4.- Coker, E.G., and Filon, L.N.G., "A Treatise on Photo-elasticity" Rev. by H.T. Jessop, Cambridge Univ. Press., 1957.

5.- Bailey, R.W., and Fidler, R., "Stress Analysis of Plates and Shells Containing Patterns of Reinforced Holes", Nuclear Eng. and Design, Vol. 3, No.1, 1966.

6.- Hulbert, L.E., and Niedenfuer, F.W., "Accurate calculation of Stress Distributions in Multiholed Plates" Trans. A.S.M.E., Series B, Vol.87, No.3, Aug. 1965.

7.- Bailey, R., and Hicks, R., "Behavior of Perforated Plates under plane Stress", Jnl. Mech. Eng. Sci., Vol.2, No.2, 1960.

8.- Fransis, H.P., and Kim, K., "A Method of Solving Certain Plane Problems of Contained Elasto-plasticity", SIAM J., Appl. Math., Vol. 15, No. 4, July, 1967.

9.- Durelli, A.J., Parks, V.J., and Feng, H.C., "Stresses Around an Elliptical Hole in a Finite Plate Subjected to Axial Loading", Trans. A.S.M.E., Jnl. App. Mechs., Vol. 33, Series E, No.1, 1966.

10.- Durelli, A.J., and Murray, W.M., "Stress Distribution Around an Elliptical Discontinuity In Any Two-Dimensional, Uniform and Axial System of Combined Stress", Exp. Stress Analysis, Vol. 1, 1943.

11.- Howland, R.C.J., "Stresses in a Plate Containing an Infinite Row of Holes", Proc. Roy. Soc. A., Vol. 148, 1935.

12.- System/360 Scientific Subroutine Package (360A-CM-03X) Version III.

13.- Timpe, A., "Die Airysche Funktion für den Ellipsenring" Mathematische Zeitschift, Vol.17.

14.- Hildebrand, B.F., "Methods of Applied Mathematics" Prentice-Hall, Inc., Enlewood Cliffs. N.J., 1965.

15.- Christiansen, S., "Numerical Determination of Stresses in a Finite or Infinite Plate With Several Holes of Arbitrary Form"